University of Alaska Fairbanks

Quarterly Research Performance Progress Report

Federal Agency and Organization Element to Which Report is Submitted	U.S. Department of Energy Office of Fossil Energy
FOA Name	Advanced Technology Solutions for Unconventional Oil & Gas Development
FOA Number	DE-FOA-0001722
Nature of the Report	Research Performance Progress Report (RPPR)
Award Number	DE-FE0031606
Award Type	Cooperative Agreement
Name, Title, Email Address, and Phone Number for the Prime Recipient	**Technical Contact (Principal Investigator):** Abhijit Dandekar, Professor, adandekar@alaska.edu 907-474-6427 **Business Contact:** Rosemary Madnick Executive Director UAF Office of Grants and Contracts Administration rmadnick@alaska.edu, 907-474-6446
Name of Submitting Official, Title, Email Address, and Phone Number	Same as PI
Prime Recipient Name and Address	University of Alaska Fairbanks Grants and Contracts Administration PO Box 757880, Fairbanks AK 99775
Prime Recipient Type	Not for profit organization
Project Title	**FIRST EVER FIELD PILOT ON ALASKA'S NORTH SLOPE TO VALIDATE THE USE OF POLYMER FLOODS FOR HEAVY OIL EOR a.k.a ALASKA NORTH SLOPE FIELD LABORATORY (ANSFL)**

Principal Investigator(s)	**PI:** Abhijit Dandekar, *University of Alaska Fairbanks* **Co-PIs:** Yin Zhang, *University of Alaska Fairbanks* John Barnes and Samson Ning, Hilcorp Alaska LLC Randy Seright, *New Mexico Institute* *of Mining & Technology* Baojun Bai, *Missouri University of Science and Technology* Dongmei Wang, *University of North Dakota*
Prime Recipient's DUNS number	615245164
Date of the Report	December 19, 2019
Period Covered by the Report	September 1 2019-November 30 2019
Reporting Frequency	Quarterly
Signature of Principal Investigator:	Abhijit Dandekar

University of Alaska Fairbanks

TABLE OF CONTENTS

LIST OF FIGURES

LIST OF TABLES

NOMENCLATURE

ANS	Alaska North Slope
BS&W	Basic Sediment and Water
bpd	Barrel Per Day
BHP	Bottomhole Pressure
BP	Budget Period
BS	Backscattering
CMG	Computer Modeling Group
cp or cP	Centipoise
DMP	Data Management Plan
EB	Emulsion Breaker
EOR	Enhanced Oil Recovery
FR	Filter Ratio
Fr	Resistance Factor
Frr	Residual Resistance Factor
f_w	Fractional Flow of Water
G'	Elastic Modulus
G''	Viscous Modulus
HPAM	Hydrolyzed Polyacrylamide
HM	History Matching
HSPF	High Salinity Polymerflood
HSWF	High Salinity Waterflood
IAPV	Inaccessible Pore Volume
ICD	Inflow Control Device
IMEX	Implicit Pressure Explicit Saturation Simulator
IPROF	Injection Profile
KI	Potassium Iodide
k or K	Permeability (generally absolute)
Kro	Relative Permeability to Oil
Krw	Relative Permeability to Water
LSWF	Low Salinity Waterflood
LSPF	Low salinity Polymerflood
md or mD	MilliDarcy
mg	Milligram
nm	Nanometer
No	Corey Exponent for Oil
Nw	Corey Exponent for Water
OIW	Oil in Water
OOIP	Original Oil in Place
PF	Polymerflood
PFO	Pressure Falloff

PMP	Project Management Plan
PPB	Parts Per Billion
PPG	Preformed Particle Gel
PPM	Parts Per Million
PRV	Pressure Release Valve
PSU	Polymer Skid Unit
PV	Pore Volume
QC	Quality Control
RF	Recovery Factor
RPM	Rotation Per Minute
SC	Standard Conditions
SCTR	Abbreviation of Sector as used in CMG
SEM	Scanning Electron Microscopy
S_{or}	Residual Oil Saturation
S_{orw}	Residual Oil Saturation due to Water
S_{orp}	Residual Oil Saturation due to Polymer
SPE	Society of Petroleum Engineers
STB	Stock Tank Barrel
STOOIP	Stock Tank Original Oil in Place
S_{wc} or S_{wi}	Connate/Irreducible Water Saturation
T_o	Oil Content in the Water Sample
TPV	Total Pore Volume
μ	Viscosity
μg	Microgram
ULSPF	Ultra Low Salinity Polymerflood
URTeC	Unconventional Resources Technology
USBM	United State Bureau of Mines
UV	Ultraviolet
VE	Viscoelasticity
VRR	Voidage Replacement Ratio
VRV	Vacuum Release Valve
WC	Water Cut
WF	Waterflood
WOR	Water Oil Ratio
XRD	X-ray Diffraction
XRF	X-ray Fluorescence

1. ACCOMPLISHMENTS

a. Project Goals

The overall objective of this project is to perform a research field experiment to validate the use of polymer floods for heavy oil Enhanced Oil Recovery (EOR) on Alaska North Slope.

The main scientific/technical objectives of the proposed project are:
1. Determine the synergy effect of the integrated EOR technology of polymer, low salinity water, horizontal wells, and conformance treatments (e.g., gels), and its potential to economically enhance heavy oil recovery.
2. Assess polymer injectivity into the Schrader Bluff formations for various polymers at various concentrations.
3. Assess and improve injection conformance along horizontal wellbore and reservoir sweep between horizontal injectors and producers.
4. Evaluate the water salinity effect on the performance of polymer flooding and gel treatments.
5. Optimize pump schedule of low-salinity water and polymer.
6. Establish timing of polymer breakthrough in Schrader Bluff N-sands.
7. Screen an optimized method to control the conformance of polymer flooding at the various stages of the polymer flooding project.
8. Estimate polymer retention from field data and compare with laboratory and simulation results.
9. Assess incremental oil recovery vs. polymer injected.
10. Assess effect of polymer production on surface facilities and remediation methods.

The technical tasks proposed in these studies focus on the following: (1) optimization of injected polymer viscosity/concentration and quantification of polymer retention via laboratory scale experiments; (2) optimization of injection water salinity and identification of contingencies for premature polymer breakthrough via laboratory scale experiments and numerical analyses; (3) reservoir simulation studies for optimization of polymer injection strategy; (4) design and implementation of a field pilot test at Milne Point on ANS; (5) identification of effective ways to treat produced water that contains polymer (including polymer fouling of heater tubes), and finally (6) the feasibility of commercial application of the piloted method in ANS heavy oil reservoirs. The project milestones, and current milestone status are shown toward the end in **Table A**.

b. Accomplishments

The primary focus of the research program, since the start of the polymer injection in August 2018, has been monitoring the performance of the pilot in the injection wells J-23A and J-24A, and production wells J-27 and J-28 respectively. In order to complement the field pilot, focus of other supporting tasks has been advancing reservoir simulation, tackling flow assurance challenges and laboratory corefloods. The accomplishments to date are summarized in the following bullet points:

- The reporting quarter has been particularly successful from the standpoint of publications resulting from the research conducted in this project. Three abstracts have been accepted for the 2020 SPE-IOR Conference scheduled for April 2020 in Tulsa, OK and one has been accepted for the 2020 SPE WRM also scheduled for April 2020 in Bakersfield, CA. Note that the acceptance rate for the SPE-IOR conference is very low, and thus the selection of three abstracts serves as the external recognition of the significance of this project. Complete citations can be found under Section 2 "Products". Currently, manuscript preparations are underway.
- Following the polymer hydration problem and hardware issues that were reported in the last quarterly as "lessons learned" that had caused a significant disruption in polymer injection; polymer injection has resumed since late August and the pilot has seamlessly continued in this reporting quarter.
- No polymer production or breakthrough has been observed more than one year after start of polymer injection, which has been monitored with both the clay flocculation and water composition analyses. Although clay flocculation test just started to show positive results, water composition analysis still could not detect presence of polymer.
- The project team is cautiously optimistic in that the incremental oil rate is estimated to be ~600 bopd (over waterflood) from polymer injection.

Since the official project start date of June 1, 2018, the entire project team has continued the practice of working meetings every other Friday for two hours to discuss the various tasks and the project as a whole. A summary of these bi-weekly meetings is provided to the project manager. Additionally, separate meetings, as needed, between the sub-groups also take place.

The following summarizes the team's progress to date in relation to the various tasks and sub-tasks outlined in the Project Management Plan (PMP):

- Task 1.0 - Project Management and Planning

Revised PMP and DMP are on file with DOE, which were submitted on April 30th 2019.

- Task 2.0 - Laboratory Experiments for Optimization of Injected Polymer Viscosity/Concentration and Quantification of Polymer Retention

Inaccessible Pore Volume. Manichand and Seright (2014) reviewed previous petroleum literature for the phenomenon of inaccessible pore volume (*IAPV*). They noted that a limited number of inaccessible pore volume values were reported in the literature, and that the range of values reported is inconsistent, considering the conditions of the experiments. One might expect *IAPV* to increase with decreasing permeability and increasing HPAM molecular weight. However, **Table 2.1** (which compares several HPAM *IAPV* values from the literature) indicates no correlation between *IAPV*, permeability and *Mw*.

Table 2.1: Literature *IAPV* values for HPAM.

Porous medium	k, md	HPAM[1]	Mw, g/mol	*IAPV*, %	Reference

Berea	49-61	Pusher 500	3 million	17-37	Dabbous 1977
Berea	761	Pusher 500	3 million	19	Dabbous 1977
Berea	90-120	Pusher 700	5 million	0-4	Knight *et al* 1974
Berea	277	Pusher 700	5 million	18.7-24	Shah *et al.* 1978
Berea	470	Pusher 700	5 million	22	Dawson & Lantz 1972
Bartlesville	2090	Pusher 700	5 million	24	Dawson & Lantz 1972
Reservoir sand	30-453	Pusher 700	5 million	32-37	Vela *et al.* 1976
Teflon	86	Pusher 700	5 million	19	Dominguez & Willhite 1978
Sand pack	12600	Flopaam 3630	18 million	35	Pancharoen *et al.* 2010

[1] All three HPAMs had 30% degree of hydrolysis.

Manichand and Seright (2014) point out that the available theories for the *IAPV* phenomenon cannot explain the magnitude and odd variations of *IAPV* with changes in permeability. It was particularly noted the average diameter of an HPAM molecule in solution (~0.5 µm) is small enough that the polymer should be able to easily fit into over 99% of the pores present in typical polymer floods (Manichand and Seright, 2014).

We found a possible explanation for the inconsistent reports of inaccessible pore volume in the literature. In particular, we suggest that previous studies used varying volumes of brine to flush polymer from the cores between the first and second cycles of polymer injection. (Determination of *IAPV* requires injection of a polymer bank, followed by a brine bank to flush out un-adsorbed polymer, followed by a second polymer bank that presumably will not experience further retention, Lotsch *et al.* 1985.) When brine displaces viscous polymer solution, viscous fingering will occur, and many (100 or more) *PV* of brine may be required to displace all free (un-adsorbed) polymer (Seright 2017). If insufficient brine is injected during this period, some of the pore space will still be occupied by free polymer that could eventually be displaced. In other words, that un-displaced polymer could be misinterpreted as *IAPV*. To investigate and demonstrate this possibility, consider **Figure 2.1**, which plots residual resistance factor versus *PV* during brine injection after polymer for two different sand packs. (In each case, the packs were 30.5-cm long, with an internal pressure tap at 15.24 cm. The reported residual resistance factors apply to the second section of the packs.) Residual resistance factor is defined as mobility during original brine injection (before polymer injection) divided by brine mobility after polymer is displaced. It is often considered the permeability reduction provided by adsorbed polymer. In **Figure 2.1**, the blue curve plots residual resistance factors during brine injection for the case of a 4100-mD NB#3 sand pack. Note that the residual resistance factor was 4 after 5 *PV* of brine and 1.6 after 100 *PV*.
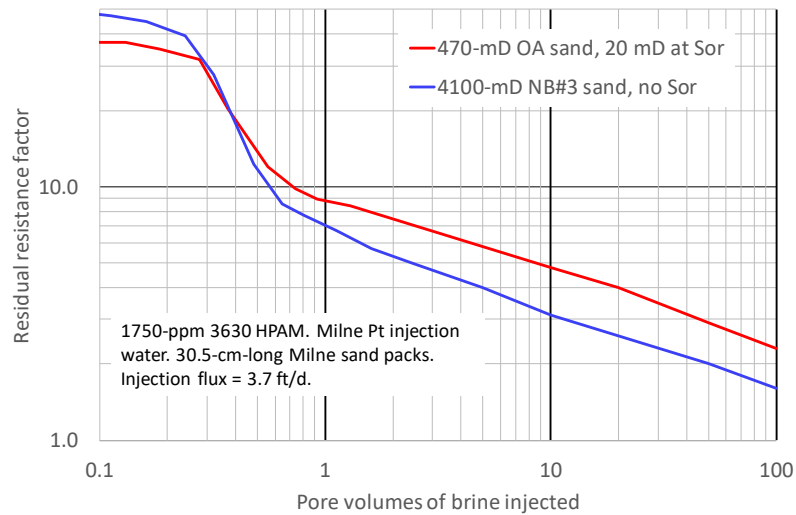
Figure 2.1: Residual resistance factors during 100 *PV* of brine injection.

In **Figure 2.2**, the polymer breakouts (as judged by nitrogen content in the effluent) are plotted for three (~5 *PV*) polymer banks associated with the 4100-mD NB#3 sand pack. The black curve shows the first polymer breakout. The blue curve was observed when a second bank of polymer was injected following a 5 *PV* bank of brine. After this second polymer bank, 100 *PV* of brine was injected. Subsequently, the red curve was obtained when a third bank of polymer was injected. Note that red curve exhibits a 50% effluent concentration at 1.00 *PV*—indicating zero *IAPV*. This finding is consistent with the earlier suggestion (Manichand and Seright, 2014) that the 0.5-µm-diameter polymer can penetrate into virtually all aqueous pore space. In contrast, the blue curve suggests that the *IAPV* after 5 *PV* of brine injection was 4%—because the 50% concentration was achieved 4% *PV* earlier than the red curve. We suggest that this apparent 4% *IAPV* value after 5 *PV* of brine is an artifact that results because mobile (un-adsorbed, un-displaced) polymer remains (because of viscous fingering). When the second polymer bank was injected, the brine viscous fingers disappeared and the 4% remaining mobile polymer saturation (from the first polymer bank) was displaced and produced. If brine had been flushed to the true residual polymer saturation, the *IAPV* would have been zero—as indicated by the red curve.

10
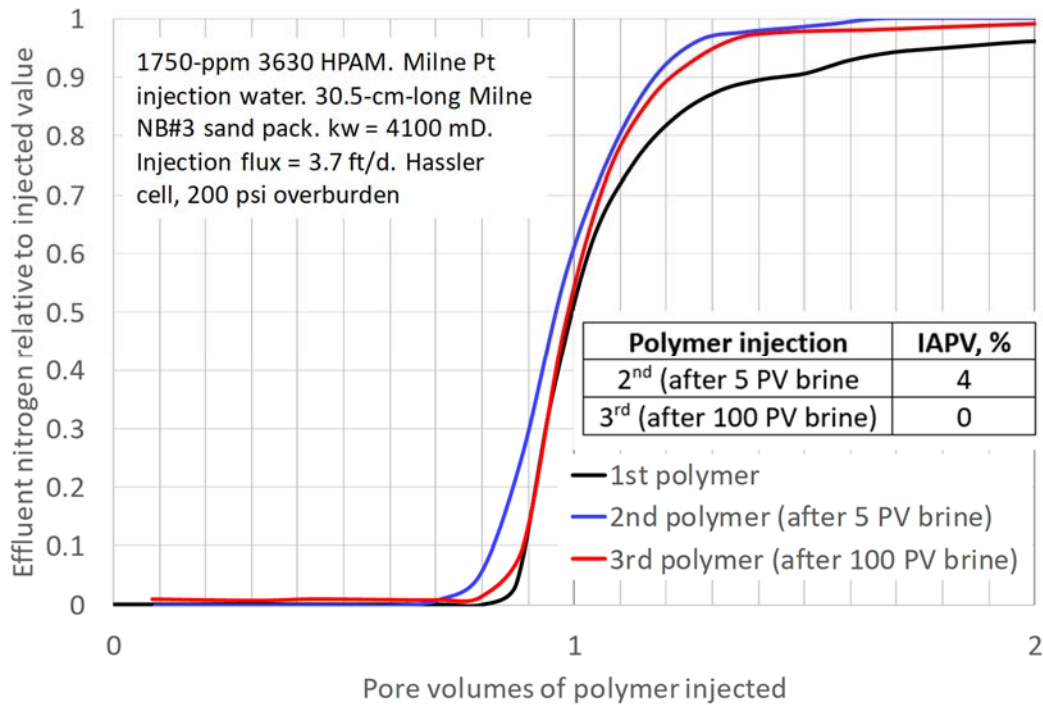
Figure 2.2: Nitrogen breakout during three polymer injections into 4100-mD NB#3 sand.

   To further test this idea, another core flood was performed involving a 470-mD OA sand pack with a confining pressure of 1000 psi. After initial brine saturation, this core was flooded to high oil saturation and then aged for 6 days at 60°C. The core was then flooded with 150 PV of brine to reach residual oil saturation. Subsequently, the core was flooded with 9.3 PV of 1750-ppm 3630 HPAM. In Figure 2.3, the black curve shows the polymer breakout, while the green curve shows the tracer breakout during the first polymer injection into this core. After polymer injection, 7 PV of brine were injected, ending with a residual resistance factor of 5.3. After this brine, a second bank of polymer solution was injected. In the blue curve of **Figure 2.3**, the 50% effluent polymer concentration level (as judged by nitrogen chemiluminescence) was reached at 0.7 PV polymer injection—suggesting that the $IAPV$ was 30%. Following this second polymer bank, 100 PV of brine were injected to drive the core to a residual resistance factor (in the second core section) of 2.3. At this point, a third bank of polymer solution was injected. For this case, the red curve in **Figure 2.3** indicates that the $IAPV$ was close to zero (because the 50% polymer concentration is reached at 1 PV). Thus, even in a porous medium with 20-mD permeability to water (i.e., 470-mD OA sand at S_{or}), the polymer appears to access all the aqueous pore space. These examples illustrate how incomplete flushing of mobile polymer solutions (during a brine post-flush) can be misinterpreted as $IAPV$. For the remainder of this work, we assume that inaccessible pore volume is zero. For field applications of polymer flooding, we support the suggestion of Manichand and Seright (2014): "A conservative approach to design of a polymer flood would assume that $IAPV$ is zero, especially in multi-darcy sands."
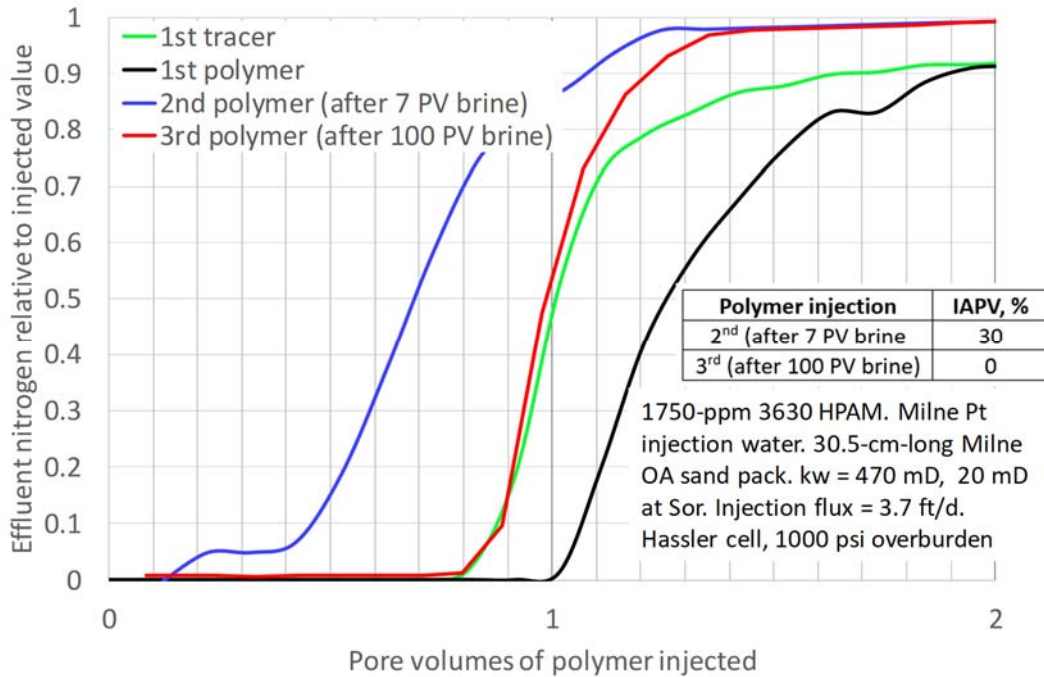
Figure 2.3: Nitrogen breakout during three polymer injections into 20-mD OA sand at S_{or}.

Polymer Retention Results. **Table 2.2** provides a summary of the polymer retention results. In all these experiments, pressure drops across the core stabilized within 2-3 *PV* of polymer injection, and no progressive plugging was observed. Resistance factors were reasonably consistent with expectations, based on viscosity measurements. Furthermore, at the end of every experiment, no polymer or gel accumulation was noted on any of the injection or production sand faces.

Table 2.2: Summary of polymer retention results.

Pack	Sand	Polymer	k_{abs}, mD	k_w at S_{or}	Core length, cm	Sand cleaned?	Confining pressure, psi	Polymer retention, µg/g
1	NB#1	3630	11250	11250	60.1	no	0	290
2	NB#1	3630	6333	--	60.1	yes	0	153
3	NB#1	3630	9240	--	60.1	yes	0	170
4	NB#1	3630	10900	7000	60.1	Greatly	0	28
5	NB#1	3630	548	50	15.24	yes	1000	240
6	NB#1	3630	625	73	15.24	yes	1700	533
7	NB#1	3430	673	116	15.24	yes	1700	236
8	NB#3	3630	4100	4100	30.48	no	200	30
9	NB#3	3630	1778	1778	30.48	no	1000	32

10	OA	3630	233	19	15.24	yes	800	126
11*	OA	3630	470	20	30.48	yes	1000	65
12	OA	3630	158	--	15.24	yes	500	87
13	OA	3630	680	--	30.48	yes	500	56
14	OA	3430	328	--	15.24	yes	1000	0

*   Pack was aged for 6 days at 60°C at high oil saturation.

Several effects were examined during our retention studies, including sand type, core permeability, residual oil, polymer molecular weight, and removal of the smallest particles from the sand. Even though the three sands (NB#1, NB#3, and OA) had similar elemental compositions, **Table 2.2** reveals that polymer retention was lowest in the NB#3 sand (ranging from 30 to 32 μg/g). The NB#3 sand had the largest particles and no particles smaller than 100 μm. In spite of being from the same layer as NB#3 (except for being located 3000 ft away), polymer retention was highest in the NB#1 sand (153-533 μg/g, except for Pack 4 where 28 μg/g was observed). In the NB#1 sand, high retention values were noted even in very permeable packs (e.g., 290 μg/g with 11250 md). The NB#1 sand had the most small particles (<20 μm). Retention values in the OA sand were intermediate (56-126 μg/g, except for Pack 14).

Prior to the retention experiment, the NB#1 sand in Pack 4 (exhibiting 28 μg/g retention) was extracted with toluene and methanol to a significantly greater extent than the other NB#1 sand packs in **Table 2.2**. This extraction process removed much more of the fine particles—explaining the low polymer retention value of 28 μg/g (red curve in **Figure 2.4**). In contrast, the NB#1 sand for Pack 1 (black curve) and the NB#3 sand for Pack 8 (blue curve) were packed in their native state (no toluene or methanol extraction). All curves in **Figure 2.4** were obtained by analyzing the sands after the retention experiment. For Pack 4 (red curve), after extensive cleaning/extraction, the pack was saturated with fresh Milne Point oil, and then drive to residual oil using 150 *PV* of brine. In contrast, for Packs 1 and 8, the native (naturally oil-coated) NB sands were packed and flooded without addition of fresh oil.

Within a given sand, polymer retention decreased modestly with increased permeability, but this correlation was not strong (**Table 2.2**). For example, in the OA sand, retention in 233-mD sand (19-mD at S_{or}) was 126 μg/g, while retention in 670-mD sand (without residual oil) was 56 μg/g.

Examination of **Table 2.2** does not definitively reveal that retention was greatly lower with residual oil present than in oil-free cores. Comparison of Packs 10 and 11 (both with k_{wsor}=19-20 mD in the OA sand) suggest that aging the core (at 60°C for 6 days at high oil saturation) may have reduced retention from 126 μg/g to 65 μg/g.

Retention of 3430 (with Mw=10-12 million g/mol) was lower than that of 3630 (with Mw=10-12 million g/mol). For example, comparing Packs 6 and 7 indicates that under very similar conditions in the NB#1 sand, retention was 236 μg/g for 3430 versus 533 μg/g for 3630. Similarly, comparing Packs 13 and 14 in the OA sands, retention was ~0 μg/g for 3430 versus 56 μg/g for 3630. Mechanical entrapment is expected to be larger as HPAM Mw increases.
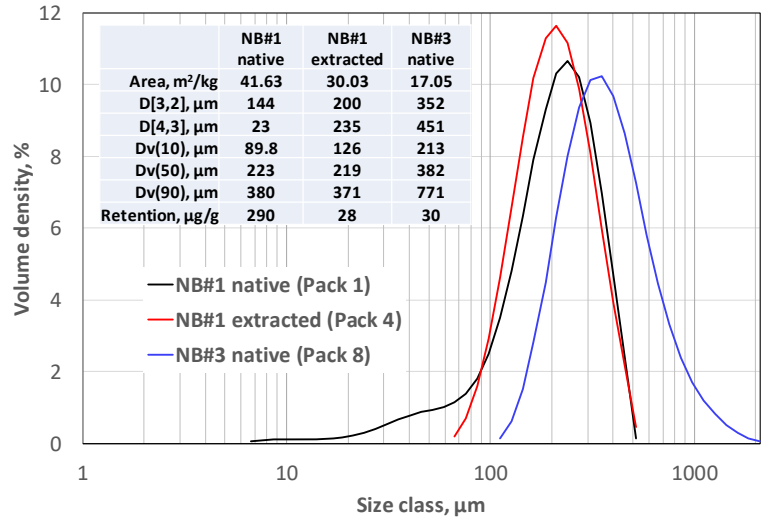
Figure 2.4: Grain size distributions for sands after retention experiments.

Slow Rise in Effluent Polymer Concentration. **Figure 2.5** indicates that in 13 of 14 retention experiments (from **Table 2.2**), the effluent polymer concentration reached 60% of the injected value before injecting 1.4 *PV* of polymer. After that point, the rise in produced polymer concentration became more gradual, depending on the particular pack. For perspective, if the effluent concentration had reached injected concentration at 1.4 PV, that would translate to a polymer retention of 88 μg/g. In other words, at least 60% of the polymer exhibits a retention value of 88 μg/g or less. The remaining polymer may exhibit higher retention—accounting for the higher retention values listed in **Table 2.2** (especially for the NB#1 sand).
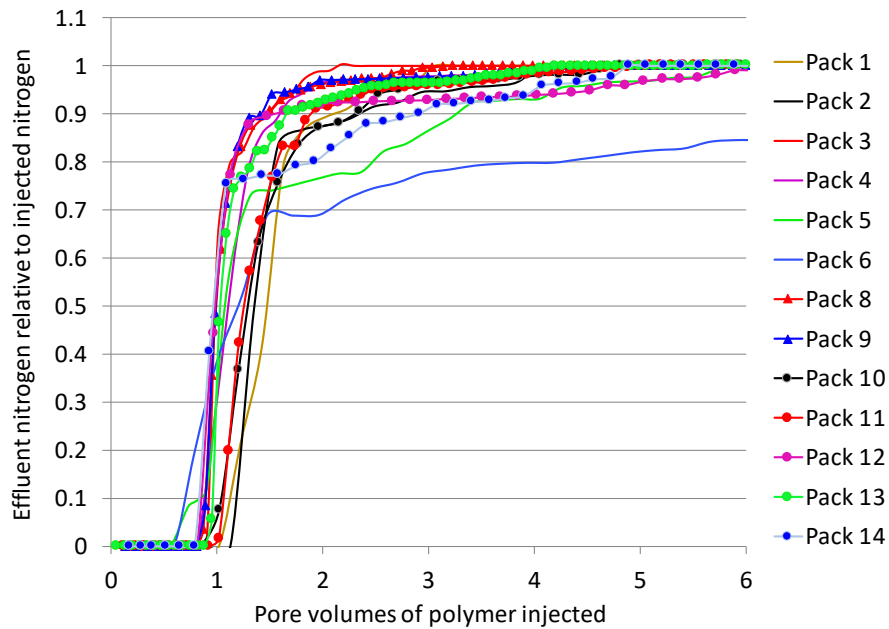
Figure 2.5: Tailing of effluent polymer concentrations.

These results imply that polymer retention was low for the first component of polymer effluent, but another component of the polymer propagates more slowly. This observation is qualitatively consistent with the model of Zhang and Seright (2014), where polymer retention was suggested to be greater at high concentrations than at low concentrations. One might suggest that this "tailing" behavior was due to high-Mw parts of the polymer molecular-weight distribution traveling more slowly through the pack than low-Mw parts. To test this concept, we monitored the zero-shear-rate viscosity during the experiments associated with Pack 8 (in **Table 2.2**) and used the method of Jouenne *et al*. (2019) to convert these measurements to intrinsic viscosities and Mw. Within experimental error, we found no change in effluent polymer molecular weight throughout the course of injecting 5.4 PV of polymer. The effluent Mw values were the same as that for the injected polymer. Thus, we could not conclude that this sand pack caused chromatographic separation of HPAM by molecular weight.

A Malvern Ultrasizer was also used in an attempt to determine if polymer size and size distribution varied with effluent throughput. However, the results revealed no detectable variations with PV throughput.

Activity is ongoing.

● Task 3.0 - Laboratory Experiments for Optimization of Injection Water Salinity and Identification of Contingencies in Premature Polymer Breakthrough in the Field

A series of coreflooding experiments were carried out in order to get a deeper understanding of the enhanced oil recovery mechanisms of polymer flooding in heavy oil reservoirs. The report includes: 1) experimental investigation of the effect of viscoelasticity of polymer solution on the oil recovery

performance; and 2) Validation of whether low salinity polymer can reduce residual oil saturation after water flooding. Moreover, preliminary experiments were carried out during this quarter to investigate the performance of gel treatment in heterogeneous reservoirs. Sand-filled fractured core models were established to mimic the channeling problem and to investigate the gel placement, plugging efficiency, and incremental oil recovery performance.

Effect of Viscoelasticity of Polymer
The Flopaam 3630 polymer shows viscoelastic behavior, which may be a main factor to improve oil recovery during polymer flooding. The viscoelastic property means the polymer solution behaves both as liquid (viscous) and solid (elastic). The viscous property of the fluid reduces its mobility in the porous media compared with water. As a result, the sweep efficiency can be improved. The elastic property of the fluid is believed to be able to mobilize residual oil that is left behind by water flooding. The viscoelastic properties of polymer solutions with different salinities were measured with a HAAKE MARS Rheometer. Basic information of the polymer solutions has been reported in previous quarter reports. The viscosities of the polymers are close to each other (around 45 cp). The salinity of the LSP is same as Milne injection source water, ~2500 ppm. The salinity of HSP is the same as Milne formation water, ~27000 ppm.

Dynamic strain sweep test was carried out to obtain the linear visco-elastic region of the polymer solutions. During the test, the frequency rate is set at 5, 10, and 20 rad/s. The strain ranging from 0.1% to 200% was scanned in order to get the linear viscoelastic region, in which the G' and G" did not change with the strain. After obtaining the linear viscoelastic region, dynamic frequency sweep test was conducted. A strain value which fell in the linear region was chosen in this test. The frequency region of 0.1-100 rad/s was scanned. The G' and G" were measured. The crossover point of G' and G" curves was obtained. At this point, the G' equals to G", which indicates the fluid transit from viscosity-dominant to elasticity-dominant at this crossover point. Three samples were tested for each polymer solution. The results are shown in **Figure 3.1 – 3.4**. For the HSP, the crossover point was at ω=11.9 rad/s. The relaxation time was 0.084s. The results indicate the HSP only shows elastic property at very high frequency of shear oscillation. For LSP, the crossover point was at ω=1.58 rad/s. The relaxation time was 0.633s. The relaxation time of LSP is eight times of HSP indicating a higher viscoelastic behavior. This may partly explain the enhanced oil recovery performance of LSP over HSP. In the following part, the two polymers are noted as High-VE polymer (low salinity polymer with higher viscoelasticity) and low-VE polymer (high salinity polymer with lower viscoelasticity).
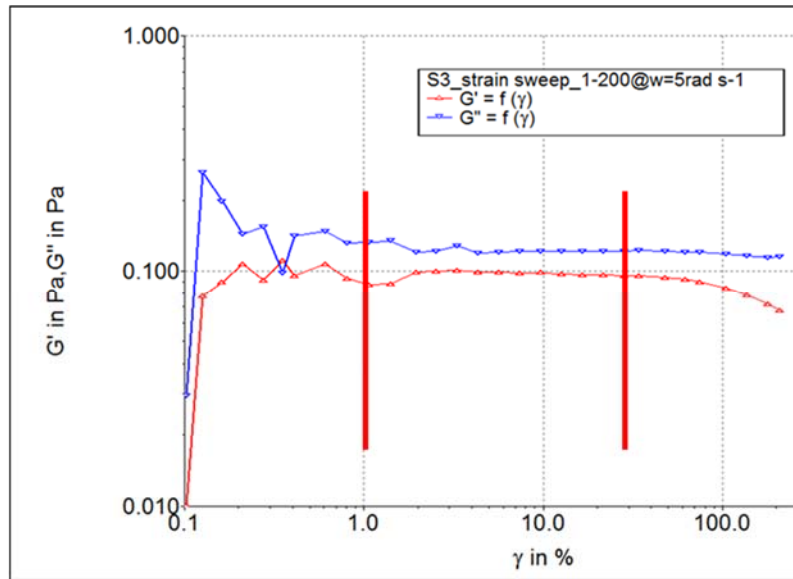
Figure 3.1: Dynamic strain sweep test result of HSP
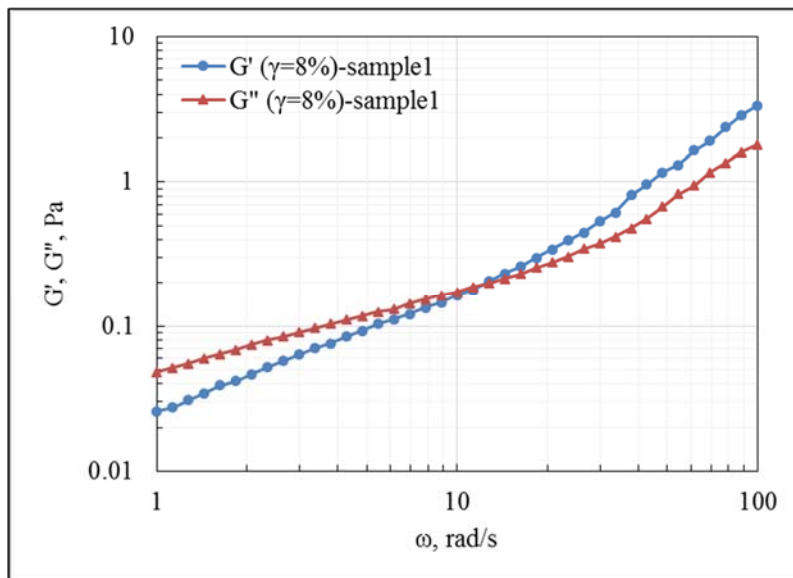
Figure 3.2: Dynamic frequency sweep test and crossover point of HSP
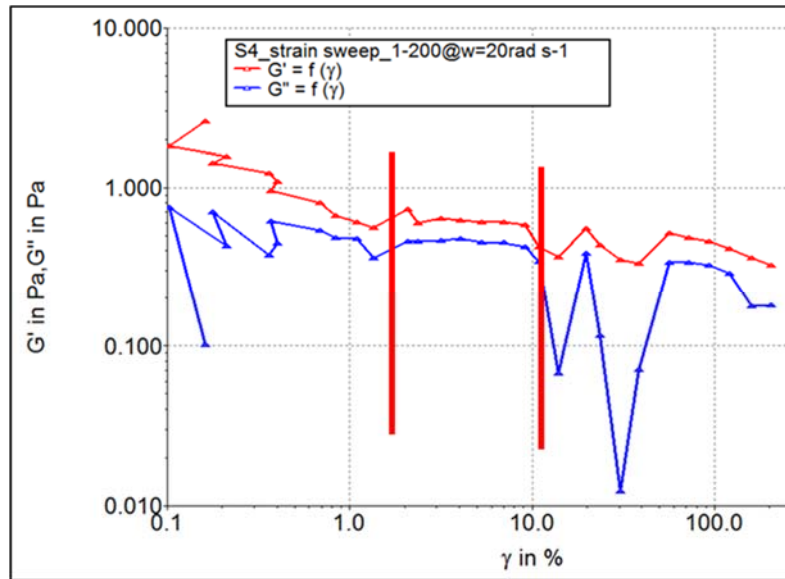
Figure 3.3: Dynamic strain sweep test result of LSP
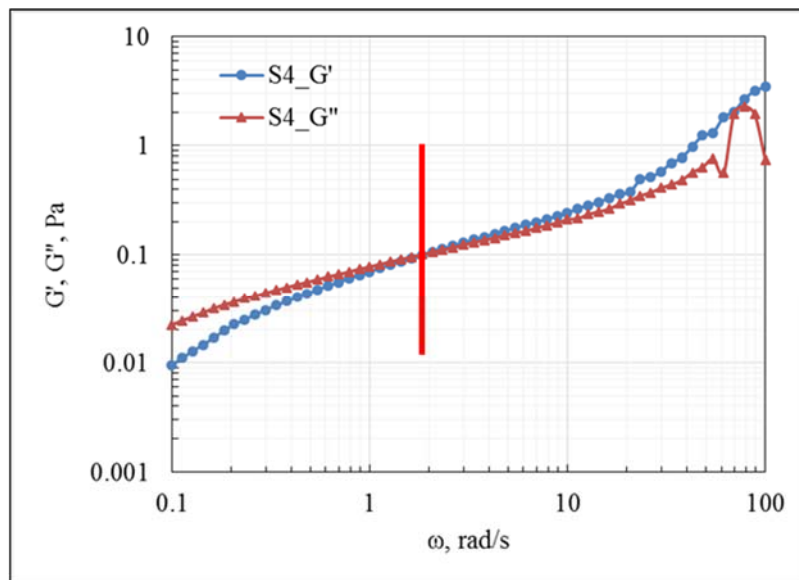
Figure 3.4: Dynamic frequency sweep test and crossover point of LSP

Coreflooding Experiments. Coreflooding experiments were carried out to investigate the displacement performance of the polymer solutions with significantly different viscoelastic properties. Due to the limited amount and poor consolidation of Milne NB formation sand, Berea sandstone cores were used in the experiments. In the future, experiments will be carried out to test whether the EOR mechanisms of polymer flooding observed in Berea sandstone cores is still valid in the target formation sand.

For the first experiment, about 3 pore volumes of synthetic Milne formation water was injected, followed

by low-VE polymer injection until no oil was produced. For the second experiment, about 3 pore volumes of synthetic Milne injection source water was injected, followed by high-VE polymer injection until no oil was produced. The cores used were twin cores that were cut from one longer core plug. Two cores had similar properties as indicated in **Table 3.1**. The confining pressure was 1000 psi. The injection rate was 0.2 mL/min (~1.9 ft/d). The injection pressure was recorded. The results are shown in **Figure 3.5** and **3.6**.

The results show that the polymer flooding with higher viscoelasticity achieved an incremental oil recovery of 19.62%, which was significantly higher than that with lower elasticity (12.28%). The former one could reduce the remaining oil saturation (or maybe the residual oil saturation) to as low as 0.207, and the latter one, however, could reduce to about 0.3. As the viscoelasticity of the high-VE polymer was significantly higher than that of the low-VE polymer, more oil left behind by water could be displaced downstream by the high-VE polymer, and thus a higher displacement efficiency was achieved. The results show the elasticity is one of major mechanisms that low salinity polymer recovers more oil than the high salinity polymer. Additionally, more research will be carried out to further investigate the effect of viscoelasticity.

Table 3.1: Basic information of the coreflooding experiments

	Low-VE polymer	**High-VE polymer**
L, cm	12.5	12.5
d, cm	2.51	2.51
Ka, mD	229	215
μ_P, cp	45	45
Relaxation time, s	0.084	0.633
Porosity	0.211	0.204
Swi	0.205	0.201
Sorw	0.392	0.363
Sorp	0.295	0.207
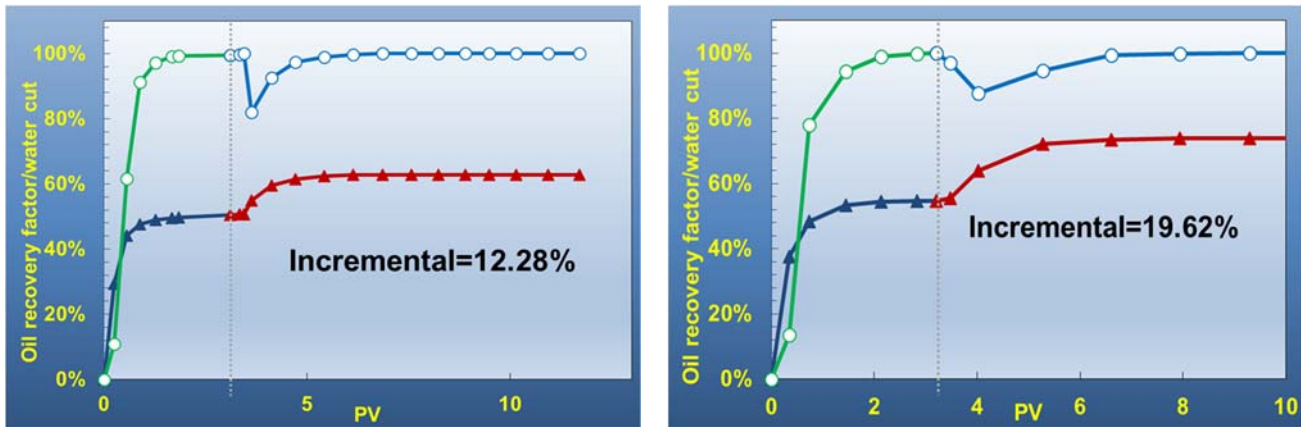
(a) Low-VE polymer   (b) High-VE polymer

Figure 3.5: Oil recovery and water cut data
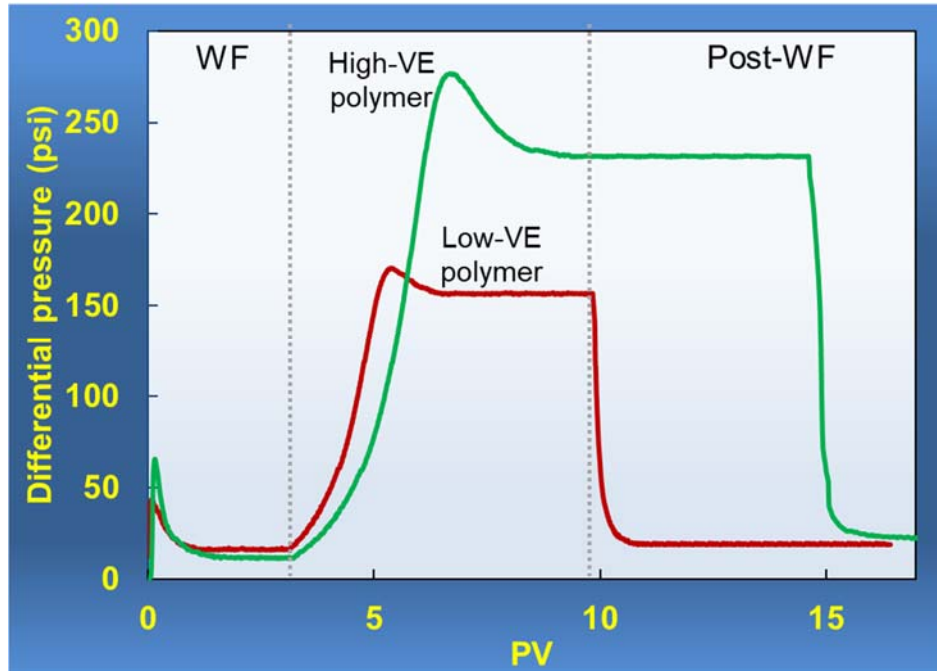
Figure 3.6: Pressure response during core flooding

The Effect of Polymer Flooding on Residual Oil Saturation (Sor)

In order to study the impact of a fluid on displacement efficiency, a true Sor (or at least an oil saturation that is very close to the true Sor) must be established to eliminate the impact of changes in sweep. Practically, a definitely true Sor is impossible to be reached, neither in laboratory nor in field, as indicated by fractional flow estimation. For heavy oil, it is more challenging to establish a theoretical Sor condition. Instead, an oil saturation close to the true Sor can be achieved with finite pore volumes of displacement practically. This endpoint oil saturation can be regarded as a reasonable residual oil saturation. Viscous glycerin solution was used to establish a reasonable water flooding Sor condition. Glycerin is a kind of

20

pure Newtonian fluid. It can be mixed with water at any ratio to get uniform solution. The viscosity of the solution reduces as the glycerin is diluted by water. In this experiment, 1-foot long Berea sandstone was used. The information of the core is shown in **Table 3.2**. The fluids used in the flooding process are shown in **Table 3.3**. The viscosity of the glycerin solution is shown in **Figure 3.7**. The result shows the viscosity of the solution does not change with the shear rate, which indicates Newtonian behavior.

The coreflooding results are shown in **Figure 3.8** and **3.9**. The endpoint mobility ratio of glycerin is 0.13, indicating a reasonable Sor was established with the high viscous glycerin solution after several pore volumes of injection. Afterwards, polymer flooding was performed. Significant incremental oil was recovered and the oil saturation in the core was further reduced, as shown in **Figure 3.9**. As the residual oil saturation was reduced, the relative permeability curve of the polymer could be affected. The polymer flooding may follow a different relative permeability curve compared with water flooding. Further research will be carried out to investigate the relative permeability of polymer flooding, which is expected to provide some guidance to lab and field scale simulation studies.

Table 3.2: The properties of the core and flood procedure

D×L, cm	Flood process	Kabs, mD (brine)	Φ	Swi
2.51 ×30.28	▪ WF (LS) ▪ GF (LS) ▪ PF (LS) ▪ post WF (LS)	688	0.245	0.262

Table 3.3: The fluid data in flooding

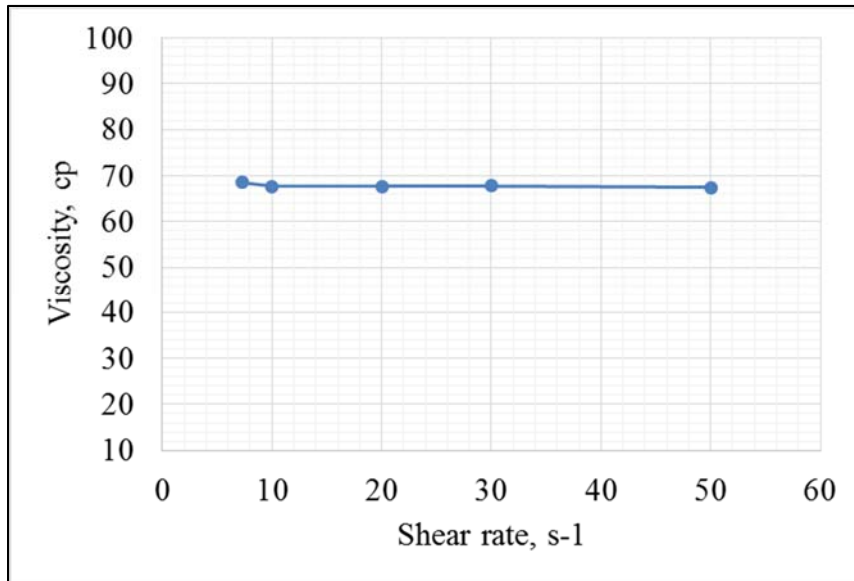| Fluid	Salinity, ppm	μ, cp
FW	27000	1.15
LSW	2500	0.99
LSG	2500	68
LSP	2500	40.8

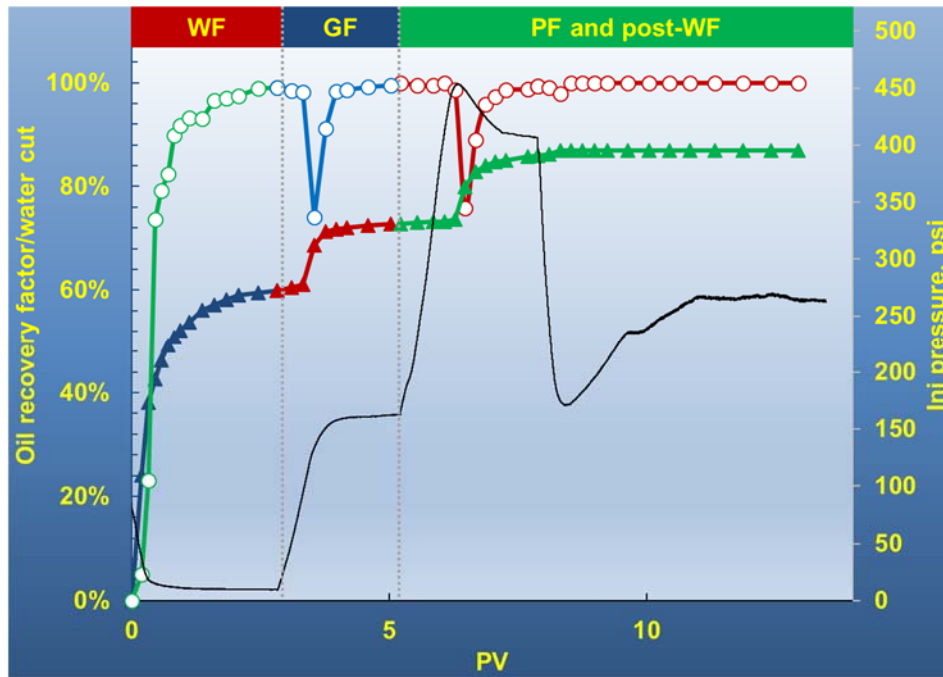**Figure 3.7: Viscosity of the glycerin solution**

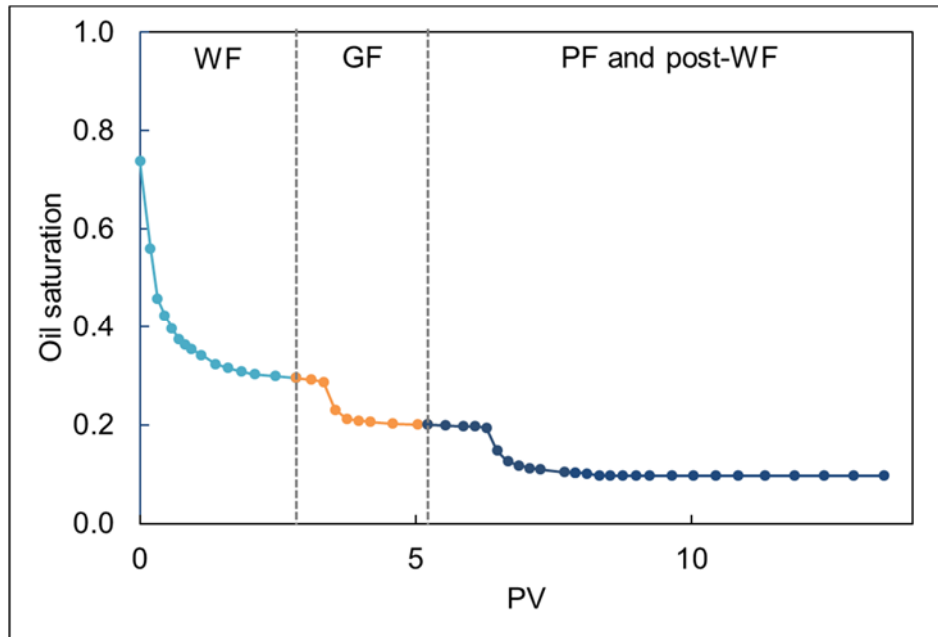**Figure 3.8: The oil recovery results and pressure response**

Figure 3.9: The oil saturation in the core during the flooding process

The Sand-filled Fractured Core Model

Presence of high-permeability channels in the reservoir will result in early breakthrough of injected water. As a result, a large portion of the oil in place is left unswept. The pre-polymer tracer test on the J pad has already shown fast breakthrough and poor sweep efficiency of water. The high-permeability streaks must be effectively blocked in order to achieve a satisfactory recovery efficiency. Though no polymer has been produced so far from both the pilot producers, one cannot conclude that no channels exist because the injected amount of polymer solution is still pretty low, less than 10% pore volume so far. Retention of the polymer in the reservoir also delays the breakthrough. On the other hand, field scale simulation has shown that high-permeability channels must be introduced into the numerical model in order to achieve a good history matching performance. Polymer, though a proven mobility control agent, may not be sufficient to significantly reduce the permeability of the channels. Additional conformance treatment is required.

Sand-filled fractured core models were established during this quarter in order to investigate the performance of gel treatment in heterogeneous reservoirs. **Figure 3.10** is the sand-filled fractured core. The preparation procedures of the model are detailed as below:
1. Drill and cut a cylindrical core sample from a rectangular core sample.
2. Saturate and cut the core sample into two half-cylindrical core samples.
3. Put two stainless steel strips (14*0.3*0.05cm) along the edge of core sample cross section, then use sand to fill the space between two stainless steel strips. The sand used was NB formation sand provided by Hilcorp.
4. Spread epoxy on both sides of stainless-steel strips to glue two half-cylindrical samples together.

5. Wrap the core model with Teflon. The parameters of the channeled model are shown in **Table 3.4**.

A couple of preliminary experiments have been attempted using the core models. The main objective of these experiments is to study microgel placement and plugging performance in the sand filled open fracture. The study includes: 1) Oil production and water cut response; 2) Buildup of injection pressure during and after PPG injected, and evaluation of blocking efficiency of the treatment to the high-permeability channel; 3) Evaluation of the damage of gel injection to the matrix; and 4) The method to remove the formation damage. The performance of some experiment runs was not satisfactory as expected. Improvement would be made in future experiments based on the lessons learned. Nevertheless, the preliminary results have shown that size selection and injection volume of the microgel were two of the key parameters to determine the success/failure of conformance treatment.
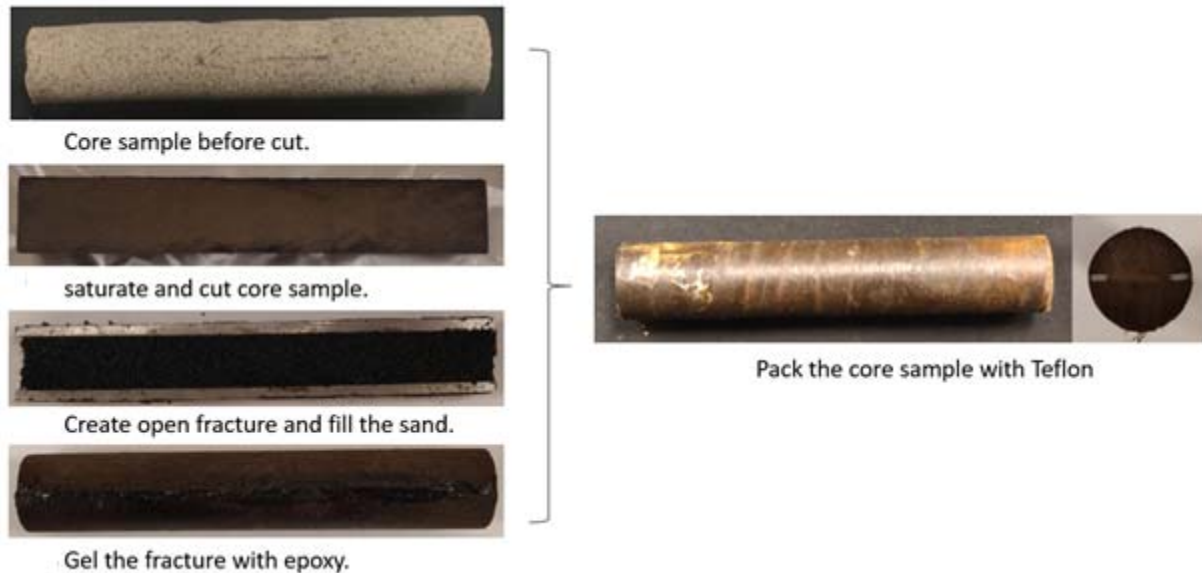
Figure 3.10: Preparation of the sand-filled fractured core model

Table 3.4: Information of the sand-filled fractured core model

Core#H41		Fracture & sand		Total	
Vb, cm3	63.45	Vb, cm3	1.40	BV, cm3	64.86
PV, cm3	14.89	FPV, cm3	0.73	PV, cm3	15.94
Porosity	0.269	Porosity	0.52	Porosity	0.25
OOIP,cm3	9.16	OOIP,cm3	0.73	OOIP,cm3	10.21
Swi	0.34	Swi	0	Soi	0.64
Soi	0.66	Soi	1	Swi	0.36
Kabs, md	506	Sand size	<80 mesh		

Summary and Further work

The experimental results demonstrate that the viscoelasticity of low salinity polymer is significantly higher than that of high salinity polymer with similar viscosity. The enhanced viscoelasticity of low salinity polymer would contribute to a higher oil recovery improvement. A reasonable residual oil saturation condition was established using viscous glycerin solution which was a pure Newtonian fluid. The favorable mobility ratio ensured a satisfactory sweep efficiency which was close to 100%. Core flooding results prove that the low salinity polymer could reduce the residual oil saturation beyond the water flooding. It indicates the polymer can improve the displacement efficiency in the water swept area. Sand-filled fractured core models were established to mimic the channeling problem and to investigate the gel placement, plugging efficiency, and incremental oil recovery performance. Preliminary results have shown that size selection and injection volume of the microgel were two of the key parameters to determine the success/failure of conformance treatment. The lessons learned would be adopted to improve the experiment design and implementation in the future.

> **Activity is ongoing.**

● Task 4.0 - Reservoir Simulation Studies for Coreflooding Experiments and Optimization of Field Pilot Test Injection Strategy

Activities and progress during this reporting quarter, completed by UND include:
- Examine how simulators with polymer functions handle polymer retention using lab-scale models.
- Core flooding history match on bottom-hole pressure behavior in two-section sand packs.
- Compare oil recovery changes versus polymer retention using field-scale models.
- Prepare outline for a paper of SPE-200428-MS along with NMT, "Polymer Retention Evaluation in A Heavy Oil Sand for A Polymer Flooding Application on Alaska's North Slope" which will be presented in the SPE IOR Conference on April, 2020 (see Section 2 "Products")

4.1 Lab-Scale Models of Polymer Retention
4.1.1 1D homogeneous simulation models for history matching polymer retention
Three polymer retention simulation models were designed based on actual laboratory core flooding conditions (under overburden pressure applied used a tri-axial core holder) using the modules of IMEX and STARS of CMG. To observe polymer dispersion visually, the models were built with 61×1×1 grid cells (instead of 31×1×1 grid blocks previously) with horizontal geometry well placements. A dummy well was placed in the center of the sand packs to simulate 2-section core flooding. Injection flux (Darcy velocity) was 3.7 ft/day for both the OA core and NB core, and various overburden pressures were applied. **Table 4.1** summarizes the parameters used in the simulation model. All parameters are consistent with the laboratory experimental data.

Table 4.1: Parameters used for polymer retention simulation of core flooding

Reservoir Parameter	Sand Pack 1	Sand Pack 2
Source formation	OA sand	NB #3 sand
Size of X – direction, cm	30.48	15.24
Size of Y – direction, cm	2.54	2.54
Size of Z– direction, cm	2.54	2.54
Pore Volume Injected, PV	6.4	5.4
Injection water salinity, ppm	2,600	2,600
Porosity, fraction	0.252	0.269
Permeability, md	680	4,100
K_{rw} at S_{or}	0	0.12
Overburden pressure, psi	500	200
*Polymer 1	3630S	3630S
Polymer concentration, ppm	1,750	1,750
Polymer viscosity, cP	44	45
Resistance factor, fraction	1	1
Inaccessible pore volume, ft^3	0	0
Initial water saturation, fraction	0	0.2

* Polymer molecular weight, 18×10^6 Daltons

4.1.2   Discussion of results

Three models based on the experiment with the OA sand were simulated using the modules of IMEX and STARS, releases of 2019. A polymer flood function through GEM/CMG was also preliminarily investigated. In this new version, all three modules can deal with polymer adsorption and EOR functions

with different individual characterizations. **Table 4.2** shows the functions described in the polymer adsorption assessments for the three modules.

Table 4.2: Major functions associated with polymer adsorption by CMG modules

Modules	IMEX	STARS	GEM
Emphasis on	Advanced wellbore modelling, black oil- based	Thermal dynamic-based	Geochemistry with a function of multiple gas components interaction with oil, EOS-based
Molecular mass of component	N/A	Required	Required
Ion exchange	N/A	Yes	Yes
Langmuir isothermal optional	Yes	Yes	Yes
Adsorption description	Normalized adsorption level vs polymer concentration	Mole fraction based	Mole fraction based
PVT function	Yes	N/A	N/A

The three modules assumed: (1) there was no ion exchange between clays and polymer solutions, (2) default polymer rheology functions (shear-thinning or shear-thickening), and (3) polymer retention was irreversible. Then the polymer retention behaviors in the core floods were examined by simulations using polymer concentration and mole fraction through polymer dispersion along the grid blocks (sand pack from injection end to production end).

4.1.2.1 Polymer retention handling in CMG/IMEX
Using IMEX module of CMG for the OA-sand experiment, **Figures 4.1a** and **4.1b** illustrate polymer dispersion at *1PV* with an injected concentration of 1,750 ppm polymer injection for various polymer retention behaviors. The table in **Figure 4.1a** lists how polymer retention was assumed to vary with concentration for four scenarios. These four cases were based on results from Zhang and Seright (2014). The polymer delayed factors noted in **Figures 4.1a** and **4.1b** were consistent with the factors estimated by Eq. 1 (from Manichand and Seright, 2014) and listed in **Table 4.3**. Thus, using the function of polymer

concentration based in IMEX, polymer retention behavior can be matched to the core flooding experimental results.
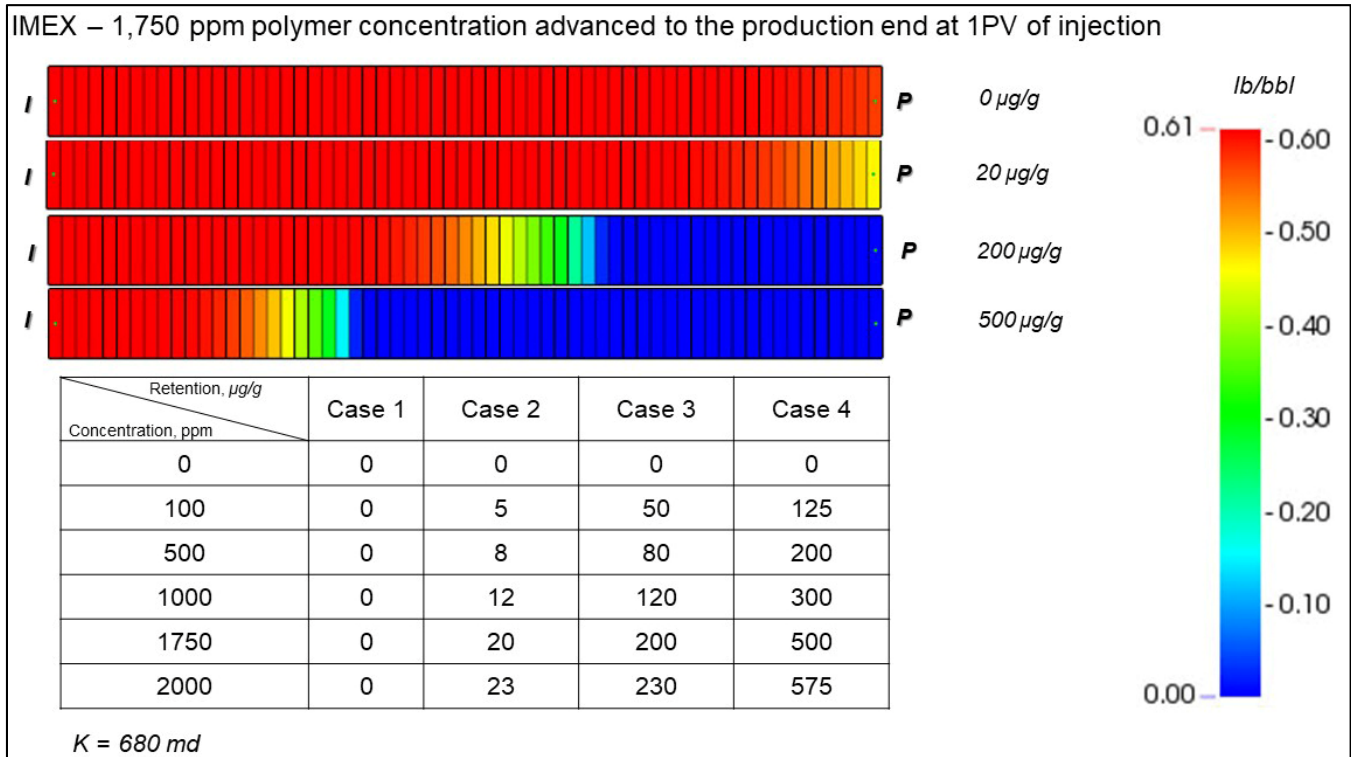

Figure 4.1a: Polymer dispersion at *1 PV* injection vs. various polymer retention values using IMEX module
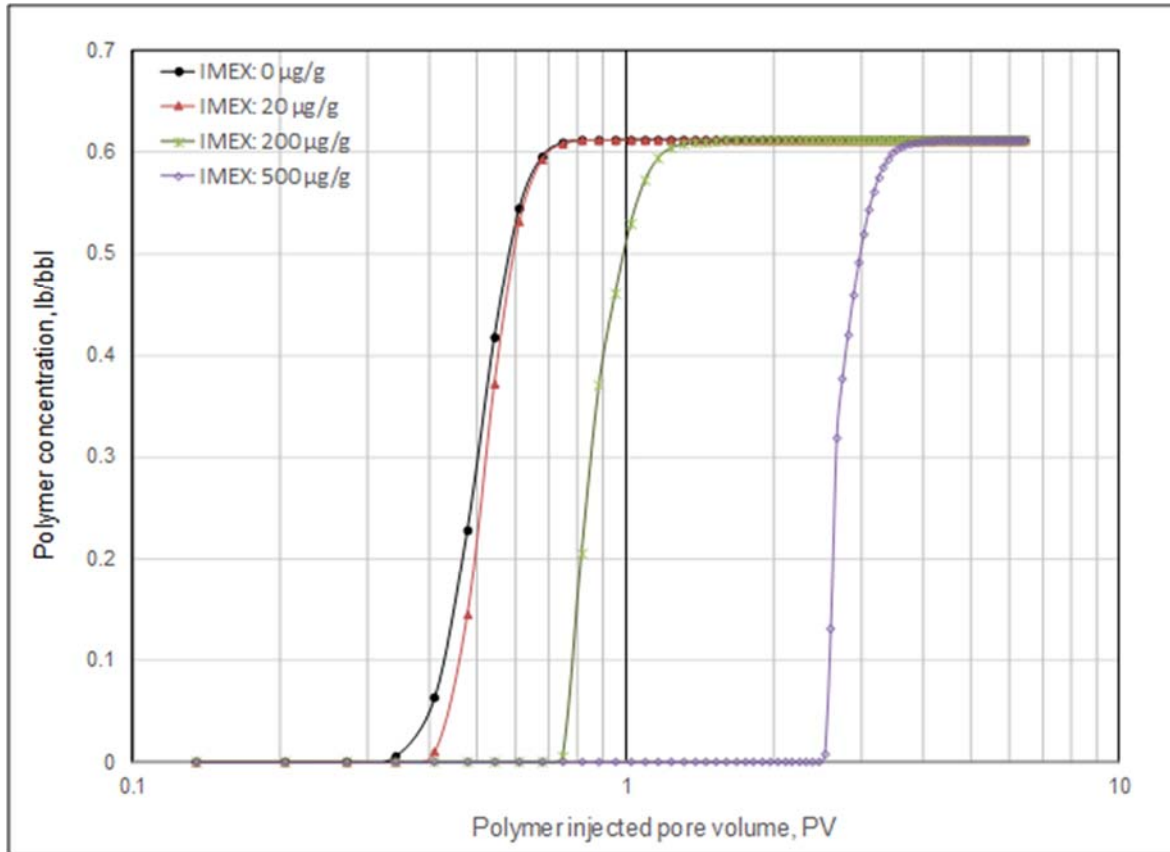
Figure 4.1b: Polymer dispersion at *1 PV* injection vs. various polymer retention values using IMEX module

$$PV_{ret} = [\rho_{rock}(1-\phi)/\phi][R_{pret}/C_{poly}] - IAPV$$

(4.1)

Where: PV_{ret} = pore volume delayed, PV; ρ_{rock} = rock density, 2.65 g/cm^3; ϕ = porosity, 0.252; R_{pret} = polymer retention, µg/g; C_{poly} = polymer concentration; $IAPV$ = inaccessible pore volume = 0.

Table 4.3: Predicted polymer delay factor: analytical model versus simulation model

Polymer retention, µg/g	0	20	200	500
Fraction of distance of polymer front through the core =1/(1+Pv$_{delayed}$)	0	92%	53%	31%
Fraction of distance of polymer front through the core through the visualization using ***IMEX***	0	91%	51%	28%

4.1.2.2 Polymer retention handling in CMG/STARS

Polymer adsorption using mole fraction input through STARS and IMEX is illustrated in **Figure 4.2**. Regardless of ion exchange, and shear-thinning or shear-thickening functions, when using the same polymer mixing function, the polymer banks exhibit little difference for the three modules. In **Figure 4.2**, the two red lines with triangles show the polymer concentrations in Grid Cell 31 from IMEX (after normalized to mole fraction). The two blue lines with dots show the polymer concentrations from STARS. The differences between the two modules were also observed in the field-scale models as shown in **Figure 4.5**.

Based on Figure 4.2, we found: (1) for a low polymer retention value of 20 μg/g, the differences of polymer advance along the sand pack between using IMEX and STARS (two solid lines) were greater than with a high polymer retention value of 200 μg/g (two dashed lines), and (2) using STARS, the polymer-advance velocity was more strongly dispersed. In other words, the polymer-advance velocities were sharper using IMEX. A possible reason of these differences might be caused by adsorption handling by the modules. In IMEX, the adsorption level (*PADSORP) is handled by the unit of pore volume with a reference porosity input (in 2019 version), as Eq 4.2 indicates. In STARS and GEM, the adsorption level (*ADMAX – STARS or *ADSORBTMAXA – GEM) are handled by a multiplier of C_f to mole fraction as Eq 4.3 shows.

$$Ad_{iIMEX} = Ad_{ilab} \bullet \frac{\rho_r(1-\phi)}{\phi}$$

$$(4.2)$$

$$Ad_{iSTARS/GEM} = Ad_{ilab} \bullet \frac{\rho_r(1-\phi)}{\phi} \bullet Cf$$

$$(4.3)$$

$$Cf = \left(\frac{1kg}{1\times10^6}\right) \times \left(\frac{(100)^3 cm^3}{1m^3}\right) \times \left(\frac{1g}{xkg}\right) = 0.125 \frac{gmol \cdot cm^3}{mg \cdot m^3}$$

Where:
Ad_{iIMEX} = Polymer adsorption level used in IMEX; g·mole/m³ or lb·mole/ft³
$Ad_{iSTARS/GEM}$ = Polymer adsorption capacity used in STARS or GEM; g·mole/m³ or lb·mole/ft³
Ad_{ilab} = Polymer adsorption tested from laboratory, mg/100g;
Cf = Convention factor;
ρ_r =   Rock density, 2.65 g/cm³;
ϕ =   Porosity; fraction
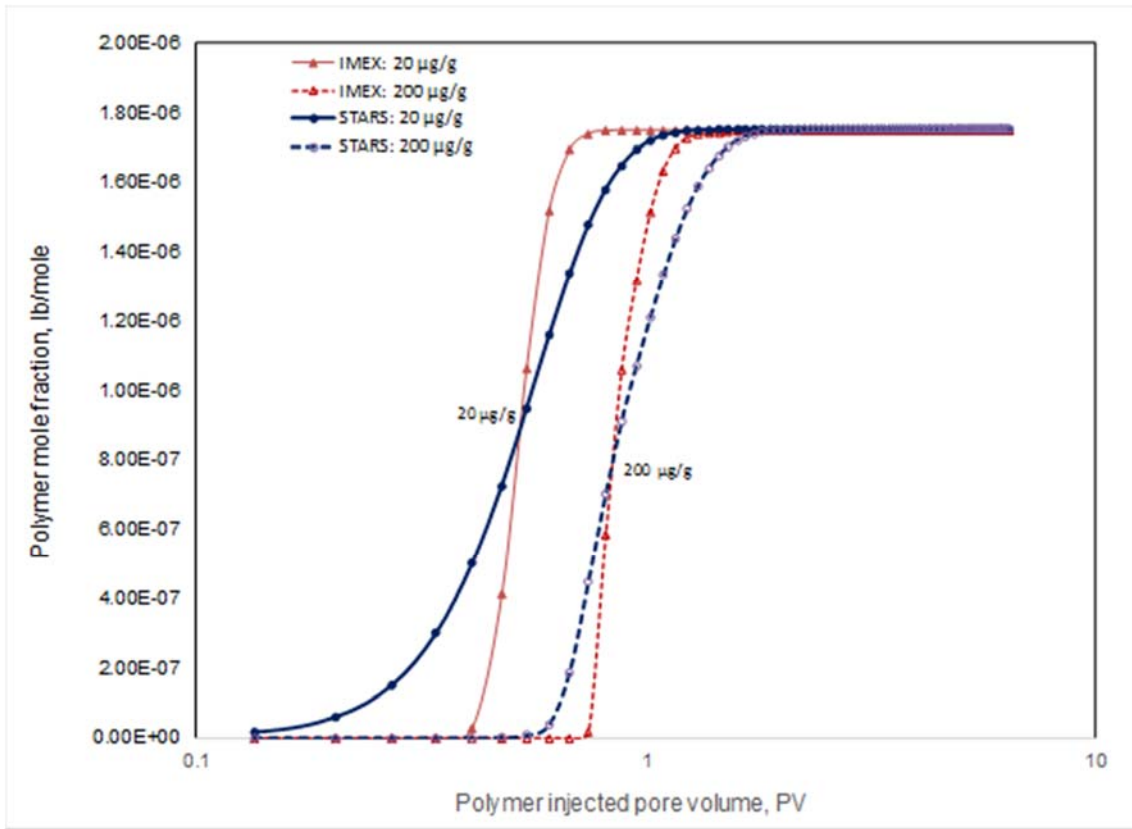x = Polymer mole mass.

Figure 4.2: Polymer dispersion comparison at *1 PV* injection and *2* polymer retention using IMEX and STARS modules

A fake molecular mass must be used in the STARS modules because the actual molecular weight of polymer of 18×10^6 Daltons will lead an extremely small polymer mole fractions (of the order of 1E-9 or 1E-10), and then lead to numerical convergence difficulties. Even though the final results by the fake molecular weight of polymer input help to prevent the numerical convergence difficulties, differences of simulation results between using IMEX and STARS still exist. But these differences may be acceptable for some analyses.

4.1.2.3 Bottom-Hole-Pressure history match on 2-section core flooding

Using IMEX, two sets of core flood results were simulated based on pressure changes. The two sand packs used OA sand and NB#3 sand. Parameters used in the simulation models are listed in **Table 4.1**. In order to simulate the pressure change in the two sections, one dummy injection well was added in the center of the model in between the injection end and production end, as **Figure 4.3** illustrates. In this case, "Injector 2" was an observation well with no actual fluid injected.

Figure 4.3: 1D model for 2-section core flooding simulation

31

Figures 4.4a and **4.4b** are the history matches on the pressure drops in the two sections when polymer advanced along the sand packs of OA and NB # 3. The dotted lines are the data obtained from actual experiments, and the solid lines are the simulation results on the pressure drops in the sections. Based on the figures, for the 1 PV injection in the Section-1s of OA and NB #3, the higher increased pressure indicated the fast polymer advancing along the core with less polymer adsorption. The lower pressure in the second core sections indicated the slow polymer dispersion when polymer advanced to the production end. The history match agreed with experimental observations.
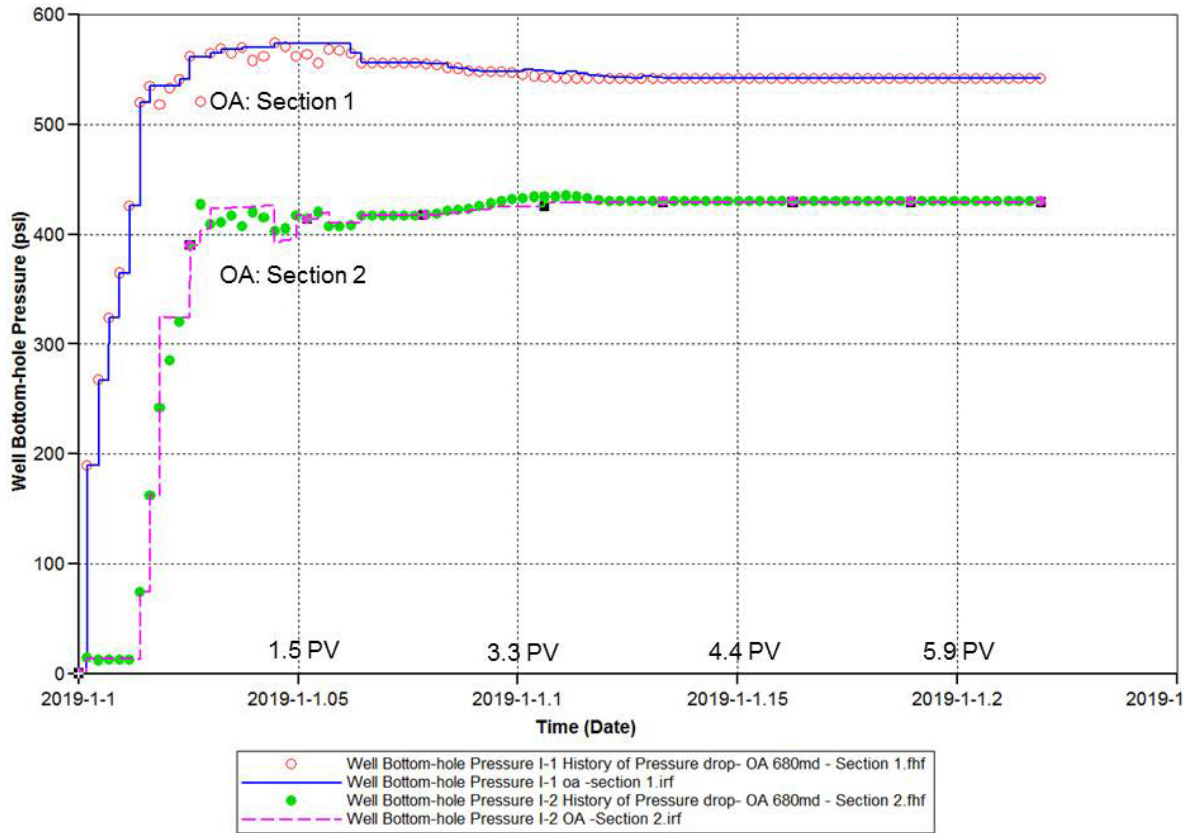

Figure 4.4a: BHP pressure history match for 2-section core flooding of OA sand
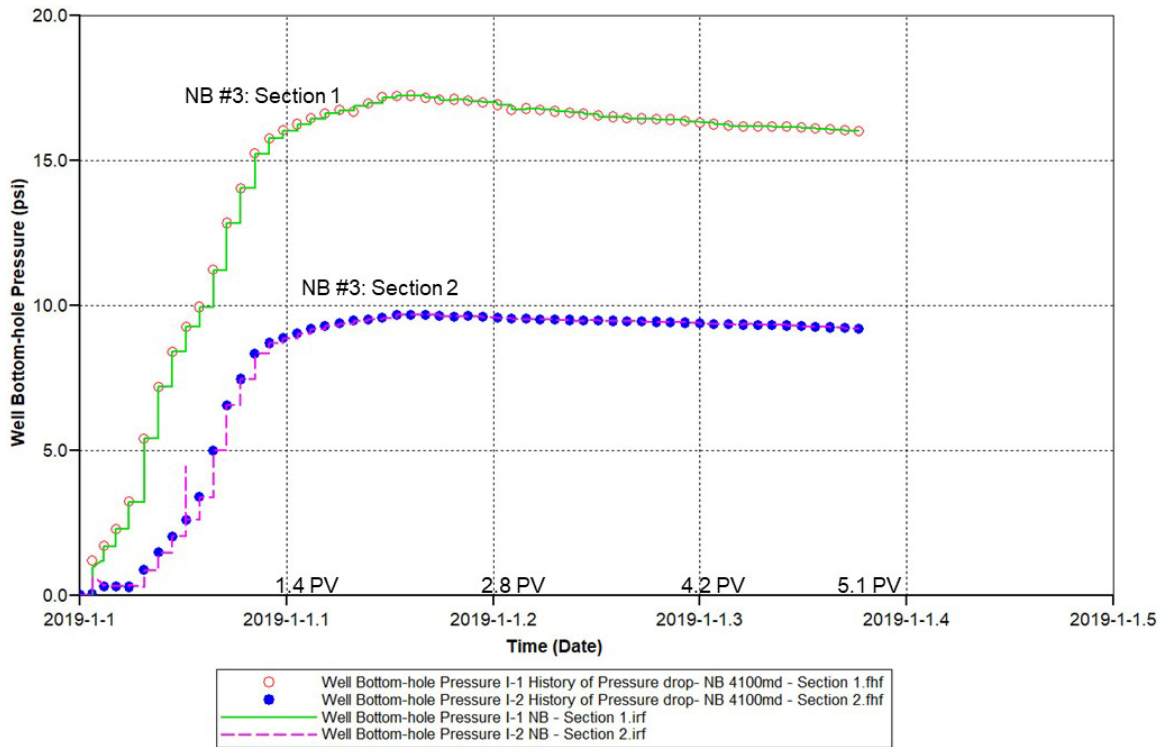
Figure 4.4b: BHP pressure history match for 2-section core flooding of NB#3 sand

4.2 Field-Scale Models of Polymer Retention

Two field-scale models for polymer effectiveness were predicted using IMEX and STARS after history match from the beginning of water flooding in the pilot to the end of July, 2019. Based on the current injection rates and production rates, polymer retention effect on oil recovery were predicted using a 10-year period of polymer injection. **Figures 4.5** shows the oil recoveries obtained at three polymer retentions (0, 20 and 200 µg/g). The plots indicate that the oil recovered at a certain period were affected by polymer retention and by different modules used.

As we observed in lab-models, similar trends were noticed in the field-scale models: (1) for a low polymer retention values from 0 to 20 µg/g, the differences of polymer advanced along to the producers between using IMEX and STARS (two black lines and two red lines) were greater compared with a high polymer retention value of 200 µg/g (two green lines) within the period of prediction, and (2) lower polymer retention led to high oil recovered. In Figure 4.5, the four solid lines were simulation results through IMEX, and the four dashed lines were the results through STARS. The two blue lines were the oil recovery factors by water flooding.
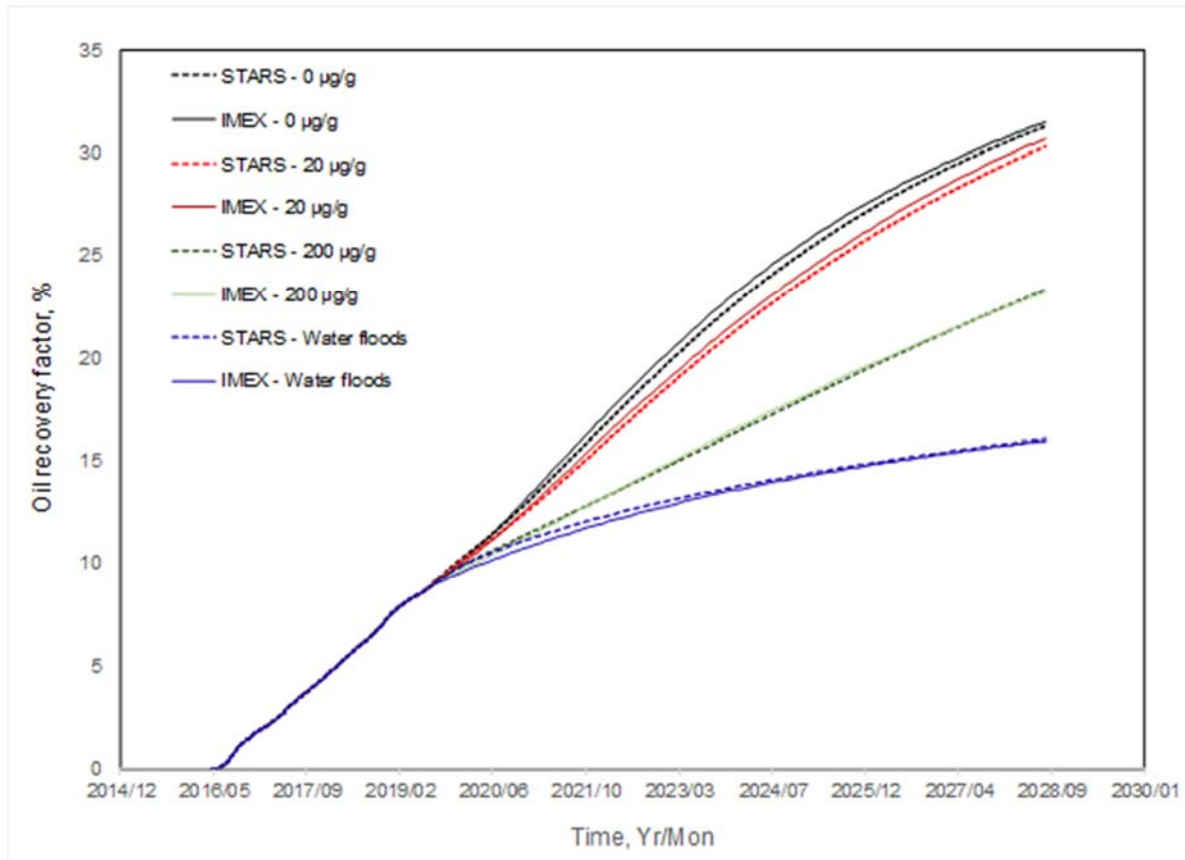
Figure 4.5: Oil recovery vs. polymer retention

4.3 Conclusions

(1) For the 1-PV injection in Section-1 of the OA and NB cores, the greater rate of pressure increase indicated fast polymer advance along the core with less polymer adsorption. The lower rate of pressure increase in Section-2 indicated slower polymer propagation. The history matches agreed with experimental observations.

(2) Inputting multiple adsorption levels (for different polymer concentrations), polymer retention can be described by two modules showing similar results as polymer propagation progresses when polymer retention was high (200 µg/g). The differences are more pronounced when polymer retention was low (20 µg/g). The above mentioned results were examined using both IMEX and STARS by field-scale model comparisons of oil recovery.

4.4 Next Plan

(1) Continue to investigate the polymer propagation function using CMG/GEM model. Especially working on WINPROP module in generating EOS model for GEM hydrocarbon geochemistry input.

(2) RRF, IPAV behavior simulation based on laboratory analysis.

(3) Paper manuscript drafting for IOR conference of 2020.

In this quarter, UAF's work focuses on investigating the effect of permeability on the production data

and introducing high permeable channels to improve the history matching results, which is reported below.

Results comparison for different simulators

A reservoir simulation model is developed in IMEX using the same model parameters (heterogeneous porosity/permeability fields, rock and fluids properties, initial conditions and well constraints) as those in STARS. The simulation results, including production data and pressure data, are compared by using two different simulators (IMEX and STARS). The oil production rates for two production wells obtained from different simulators are shown in **Figure 4.6**. The solid line represents the simulation result using IMEX, and the dash line is the simulation result using STARS. It can be seen that the same result is obtained from two different simulators by using the same model parameters. Similarly, the simulated pressure data of injection wells and production wells is the same for two different simulators. Then the permeability is tuned in history matching the production data by using IMEX.
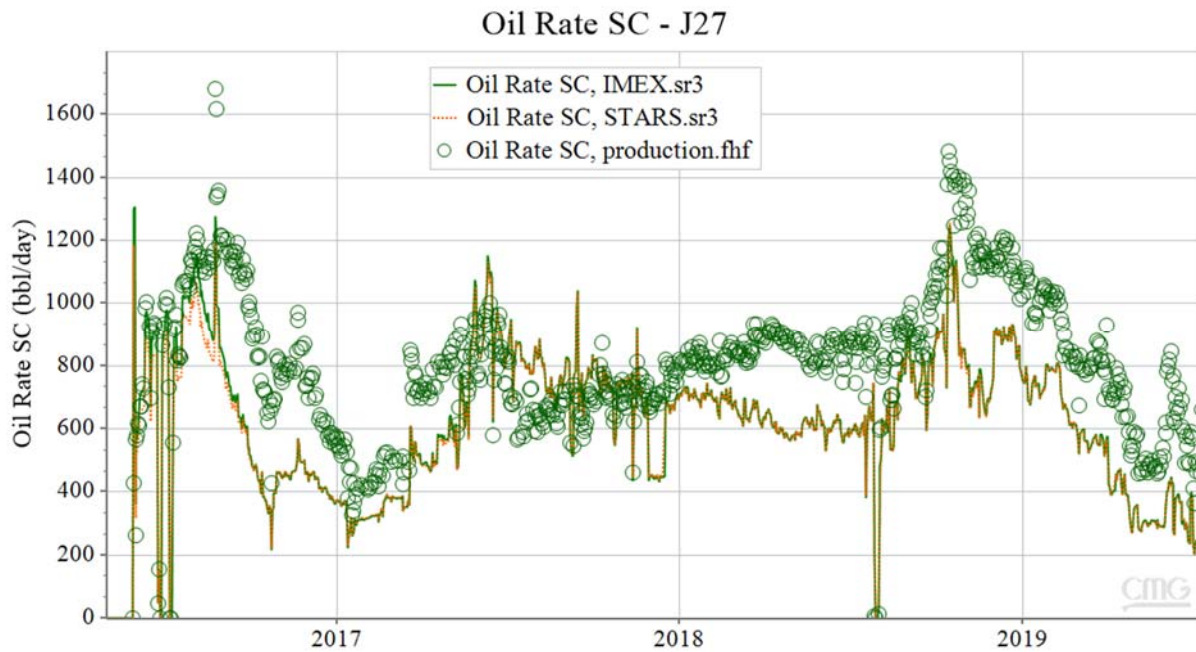
(a) Oil production rate of producer J27
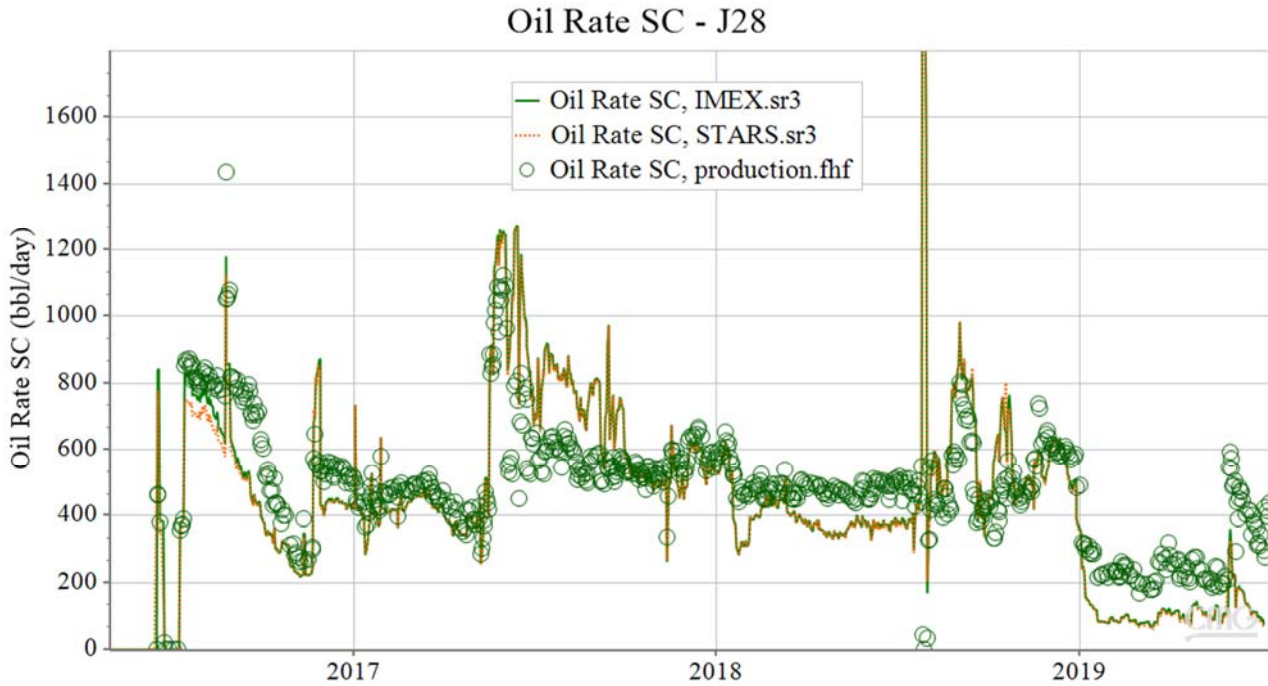
(b) Oil production rate of producer J28

Figure 4.6: Simulation results of oil production rate for two producers

The effect of permeability

To investigate the effect of permeability on production data, different types of permeability distribution (layer-cake, blocks/stripes and heterogeneous field) are employed in the reservoir simulation models. The permeability of each layer in layer-cake model and blocks/stripes model is initially assigned with the average permeability of the corresponding layer. Then the permeability in these models is tuned between 100 and 10000 mD to history matching the oil production rate and water cut. The estimated permeability fields are presented in **Figure 4.7**.
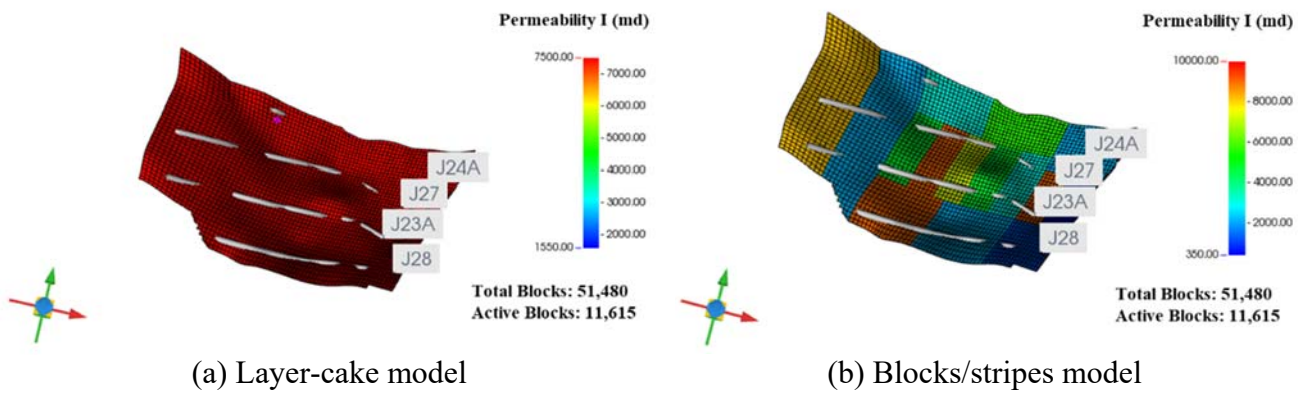
(a) Layer-cake model

(b) Blocks/stripes model
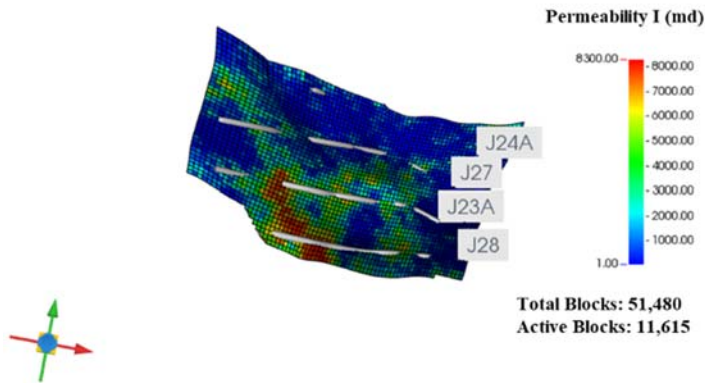
(c) Heterogeneous model
Figure 4.7: Different types of permeability distribution in the simulation models

The optimal history matching results of water cut for two production wells are shown in **Figure 4.8**. The blue line is the simulation results using layer-cake model, the green line represents the simulation results obtained from blocks/stripes model and the grey line is the simulation results using heterogeneous model. The dots are the actual production data. It can be found that the simulated water cut curves of two production wells are significantly different from the actual production data from May 2017 to January 2018 no matter which model is used. That is, using different types of permeability field has less effect on improving the history matching results.

(a) Water cut of producer J27
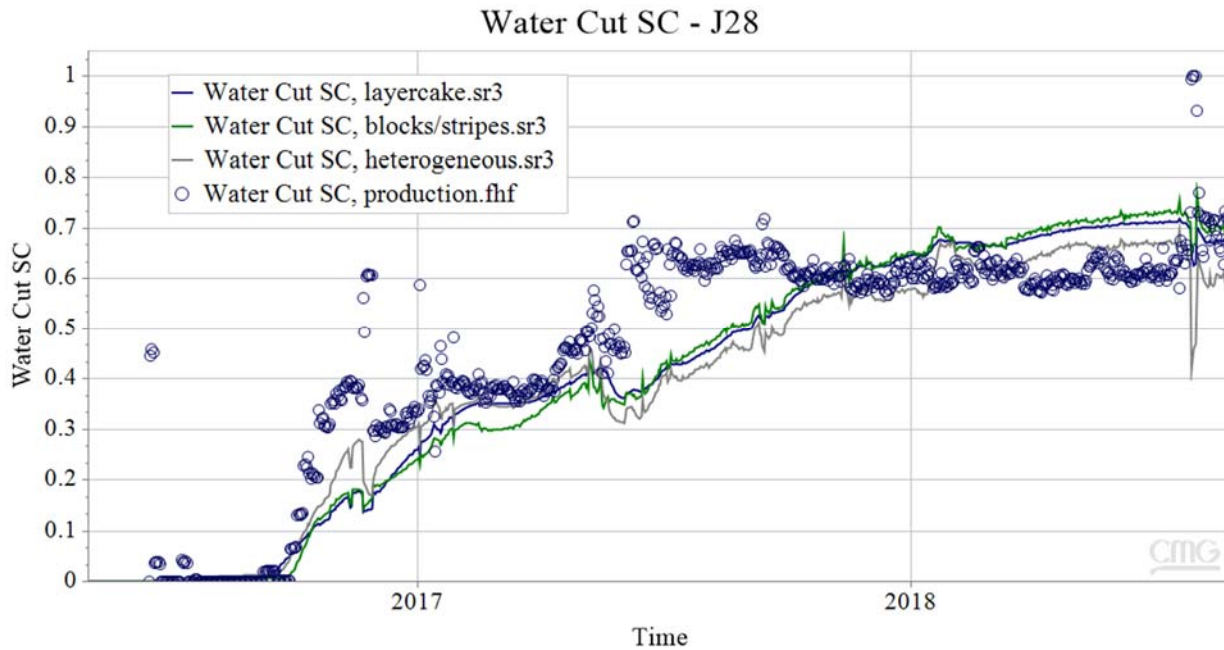
(b) Water cut of producer J28
Figure 4.8: Simulation results of water cut for two producers

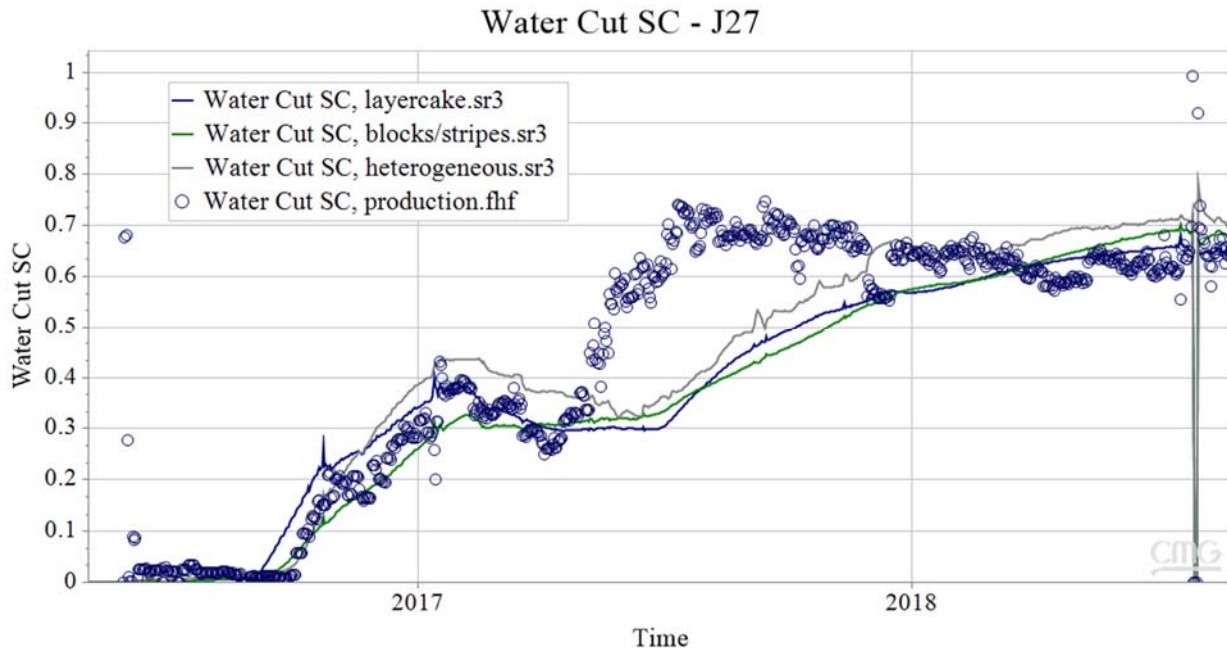Compared with the simulation results, the water cut of two production wells in the oil field increase sharply from May 2017. Meanwhile the water injection rate of injector J23A increases from 1200 to 2000 bbl/day and the water injection rate of injector J24A increases from 900 to 1800 bbl/day. Considering that the reservoir formation is unconsolidated structure, high permeable channels may have been generated between injection and production wells due to the increase in the injection pressure and/or rate. So the injected water can flow quickly to the production wells through these high permeable channels. Then several high permeable channels are introduced to the simulation model and the permeabilities of these channels are tuned to history matching the production data and tracer test data.

Simulation model with high permeable channels
When the water injection rate increases, the particles and sand will migrate and high permeable channels can be generated in the unconsolidated reservoir formation. However, the permeability of these channels will decrease when the injection rate decreases or remains unchanged. So the permeability of channels will change with time. During the simulation process, the fluid transmissibility between grid blocks is proportional to a cross-sectional interblock flow area, an averaged permeability value and a divisor equal to interblock distance. The fluid transmissibility multiplier can be tuned with time to simulate the changing permeability. To obtain better history matching results, two high permeable channels are set between the adjacent injection and production wells in the heterogeneous model, resulting in six channels in total, as shown in **Figure 4.9**. The production wells are constrained to the oil production rate. The transmissibility multipliers and widths of the channels are tuned manually to history matching the water cut and tracer mass rate.
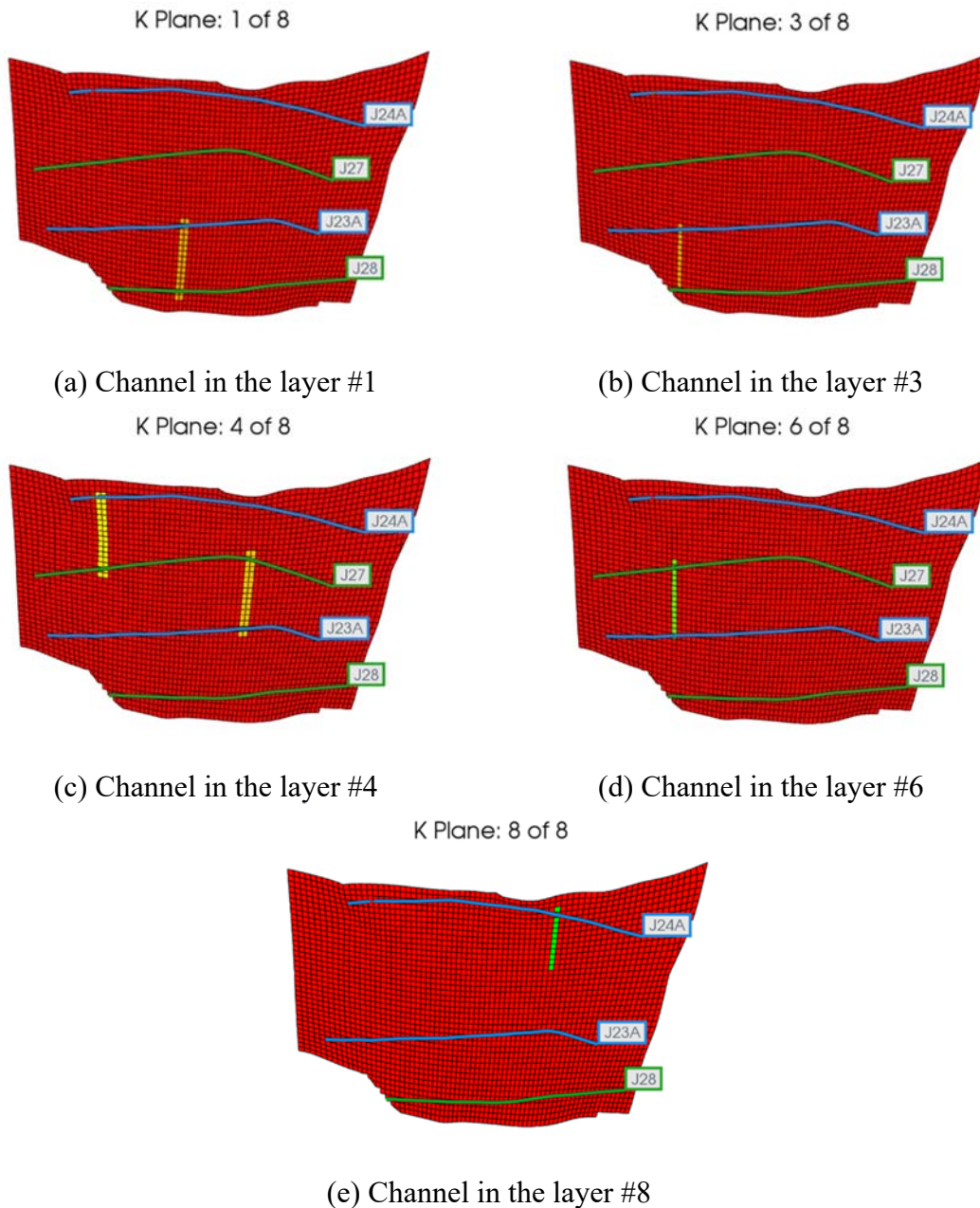
K Plane: 1 of 8

K Plane: 3 of 8

(a) Channel in the layer #1

(b) Channel in the layer #3

K Plane: 4 of 8

K Plane: 6 of 8

(c) Channel in the layer #4

(d) Channel in the layer #6

K Plane: 8 of 8

(e) Channel in the layer #8

Figure 4.9: Location of high permeable channels in the simulation model

History matching results

The optimal history matching results of water cut for two production wells are presented in **Figure 4.10**. It can be seen that the simulated water cut increases rapidly from May 2017 and is consistent with the actual production data for two production wells. Employing simulation model with channels and altering the permeability of channels with time can improve the history matching results. This verifies that the

high permeable channels can be generated in the reservoir formation.
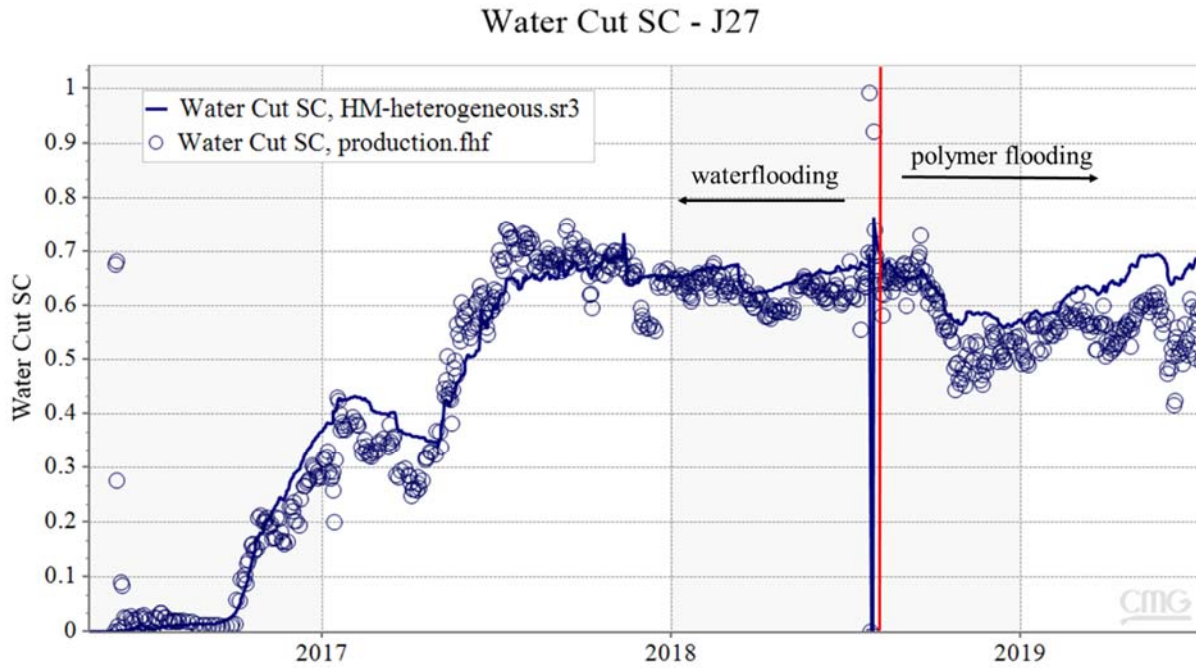
(a) Water cut of producer J27
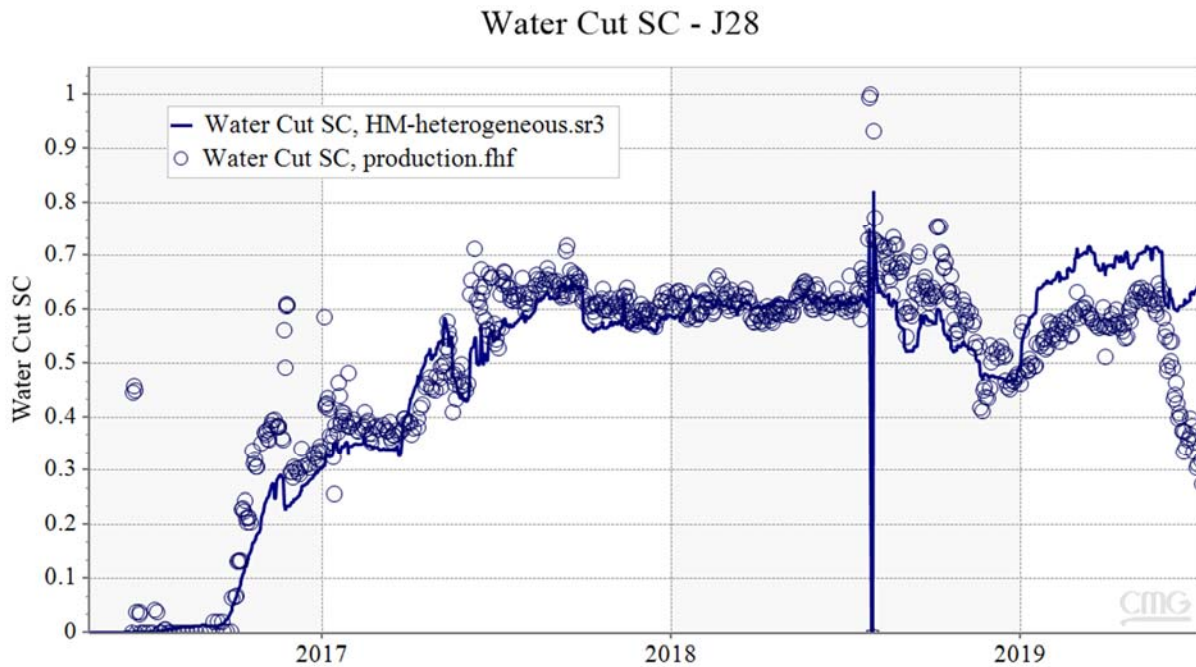
(b) Water cut of producer J28

Figure 4.10: History matching results of water cut for two producers

The history matching results of tracer mass rate in producer J27 and J28 are shown in **Figure 4.11**. It can be found that the simulated tracer breakthrough time agrees with the tracer test data, and the trend of tracer mass rate is consistent with the observation data. In general, the simulation results have been improved by tuning the permeability and the width of these channels.
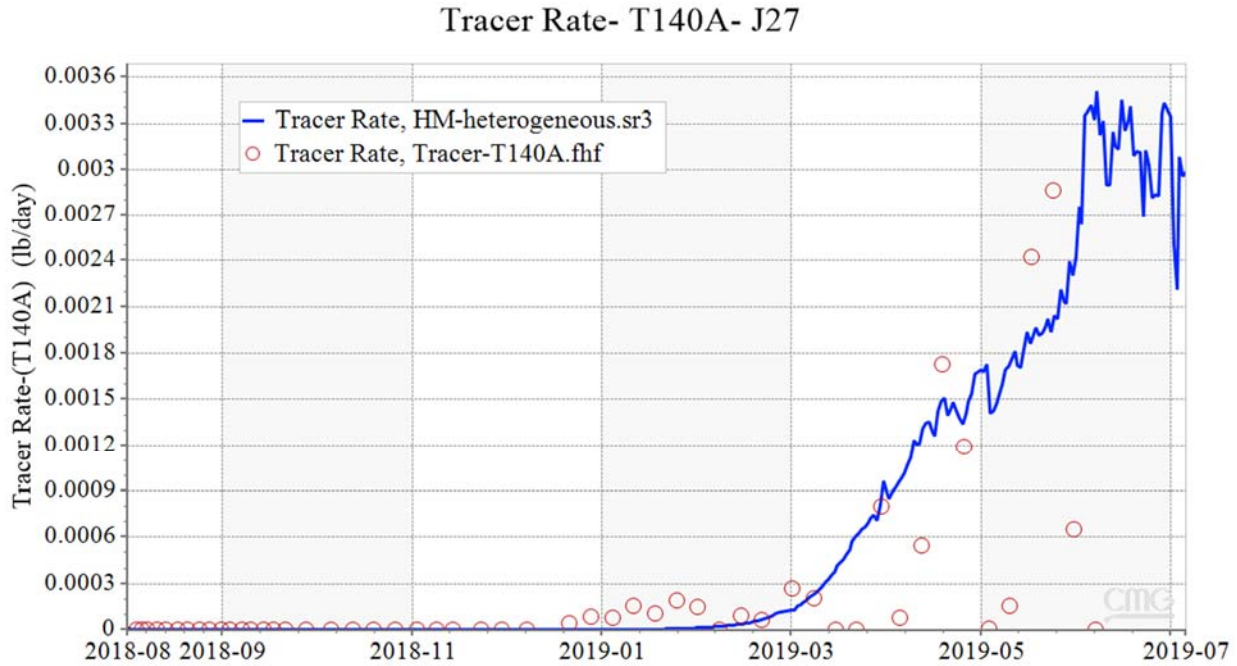
(a) T140A mass rate in producer J27

Tracer Rate- T140C- J27
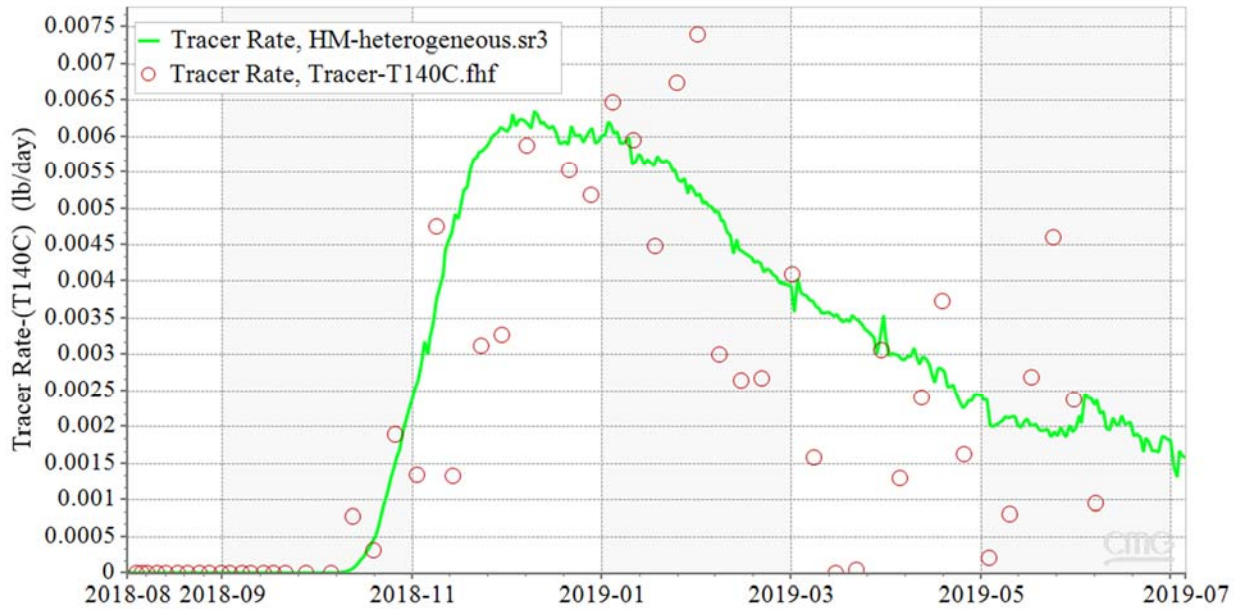
(b) T140C mass rate in producer J27

Tracer Rate- T140A- J28

(c) T140A mass rate in producer J28

University of Alaska Fairbanks

(d) T140C mass rate in producer J28
Figure 4.11: History matching results of tracer mass rate in two producers

UAF's future work will focus on the sensitivity analysis using the updated reservoir simulation model. The effect of injection rate, polymer concentration and retention on the oil recovery will be discussed. Then the operation parameters will be optimized to enhance the oil recovery economically.
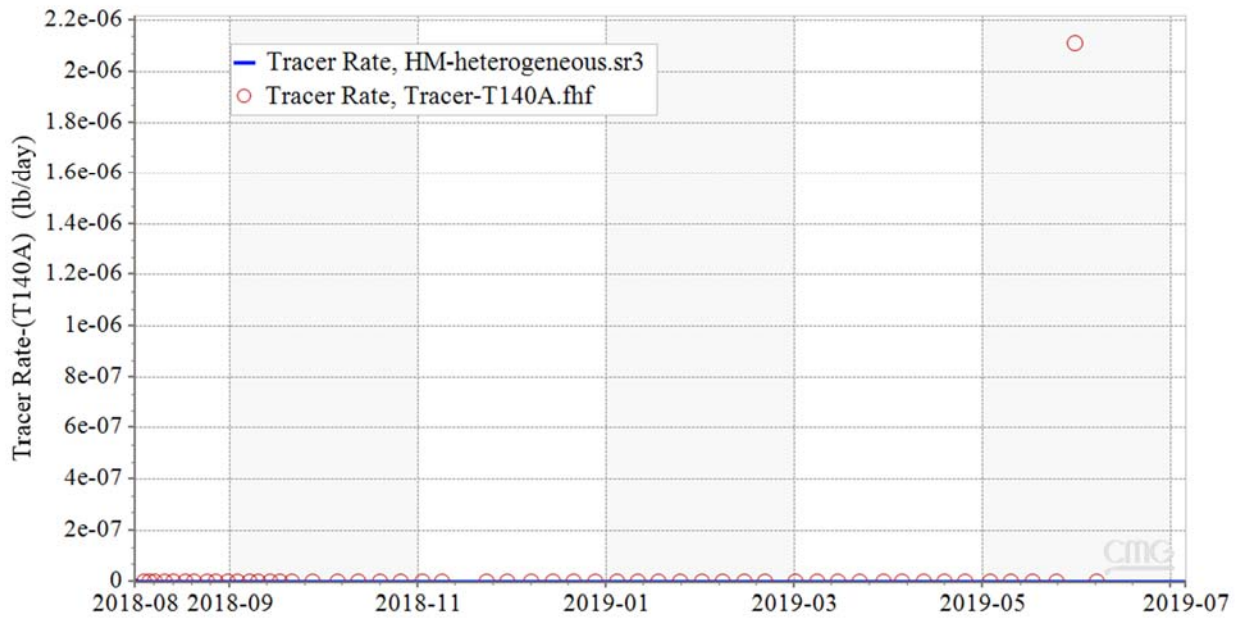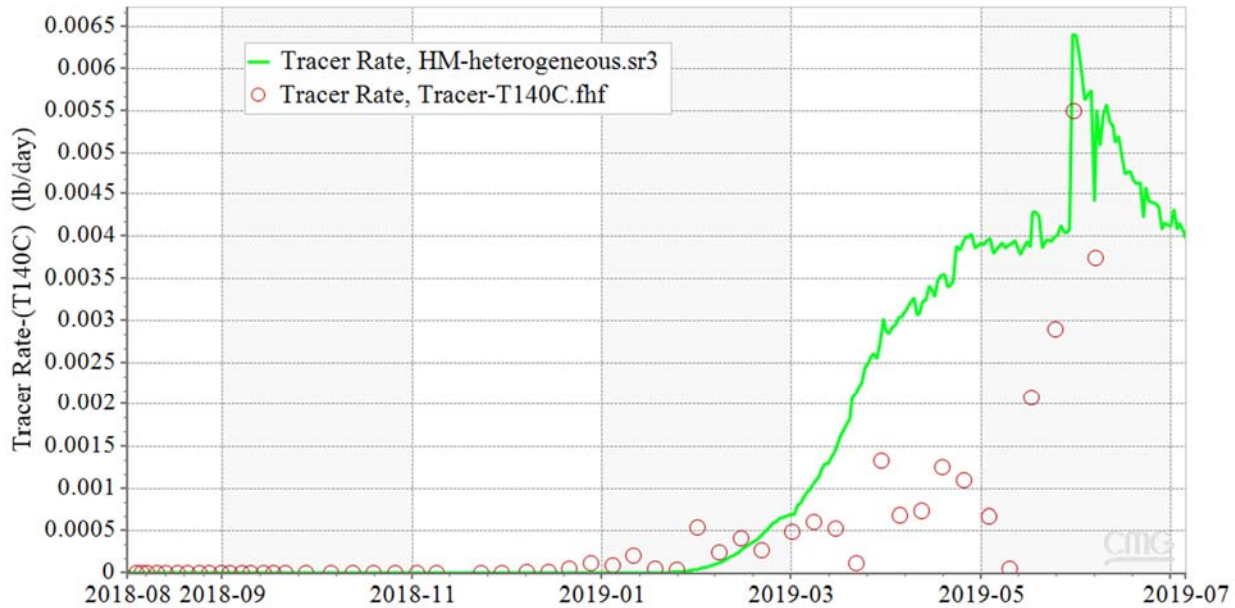
Both UND and UAF activities are ongoing.

● Task 5.0 - Implementation of Polymer Flood Field Pilot in Milne Point

Polymer injection into the two horizontal injectors (J-23A and J-24A) started on August 28th, 2018. There were two shutdowns in 2018 due to necessary equipment modifications and repairs, one in September and another in November. Then from mid-June through late-August 2019, polymer injection was interrupted due to polymer hydration issues. After 2 months of hard work by the Milne Point team assisted by SNF staff, the polymer hydration problem has been resolved and normal polymer injection has resumed since August 29th, 2019. Ultimately as a team we have learned a lot about polymer, polymer facilities and onsite QC required.

Detailed pilot activities are summarized below:

Polymer Injection Status Timeline
  • 8/23 polymer skid (PSU) online with water
  • 8/28 polymer injection starts

- 9/25 PSU shutdown
  - More HC gas found in SW
  - Need to modify and reclassify PSU to Class I Div II
- 10/15 Resume polymer injection
  - Ran downhole gauge
  - Performed post polymer step rate test
- 11/9 J-23A shut in for PFO while waiting for pump repair
- 11/16 J-24A shut in for PFO while repairing augur
- 12/3 Resume polymer injection
- 1/17/19 Attempted IPROF for J-23A, but tool covered by black goo
- 3/28/19 Pumped 8 kg Tracer T-801 into J-24A
- 3/29/19 Pumped 8 kg Tracer T-803 into J-23A
- 3/29/19 Coil tubing clean out J-23A, repeat IPROF.
  - Tool did not go all the way down, got partial results
  - ICD#1=5.6%, ICD#2=27.8%, ICD#3=40.7%
  - 74% polymer injecting into first segment (heel-2766')
- 6/7/19-6/14/19 J-28 false polymer positive by flocculation test
- 6/19/19 shut down PSU due to polymer hydration issues
- 6/22/19 PSU back online, J-23A rate decreased by 400 bpd, J-24A by 200 bpd
- 7/6/19 J-23A PFO test, no damage identified
- 7/8/19 Treat injectors with hot KCL water to remove damage – not effective
- 7/15/19 J-23A and J-24A step rate test
- 7/18-8/28/19 straight water or low concentration polymer while diagnosing
- 8/29/19 polymer hydration problems resolved, resume polymer injection
- 9/2/19 J-23A and J-24A step rate test

Polymer Injection Performance

Injectivity of J-23A and J-24A apparently decreased after a 5-day shut in in mid-June. A pressure falloff (PFO) test was performed on J-23A early July to assess the apparent formation damage. However, the PFO results did not indicate severe skin damage. Step rate tests were performed in early September on both injectors to assess the injectivity and fracture pressure. Here are the main observations from the step rate test analysis:

1. All data fall on a straight line for both wells, indicating no formation break down during the test.
2. Injectivity index is fairly high in both wells (5 bpd/psi for J-23A and 3.6 for J-24A) indicating that the sand is already fractured/parted at the lowest injection rate.
3. Results of the step rate and the PFO tests show no signs of skin damage to the injectors. The reduced injectivity might be just caused by the high viscosity polymer solution propagating through the reservoir.
4. It seems that we just have to increase injection pressure to achieve higher target injection rate.

As of November 30, 2019, cumulative polymer injected was 350,000 lbs into J-23A and 149,000 lbs into

J-24A. During the reporting period, injected polymer concentration was between 1450 to 1800 ppm to achieve a reduced target viscosity of 40 cP as shown in **Figure 5.1**.
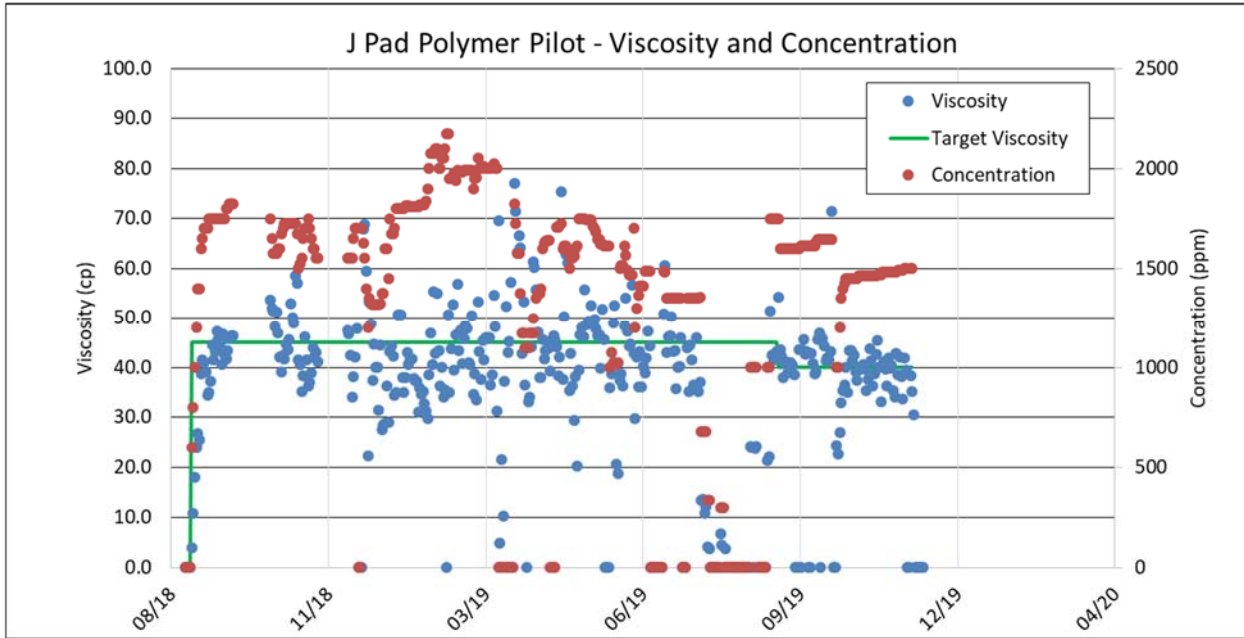
Figure 5.1: Polymer concentration and viscosity vs. time.

Figure 5.2 presents daily injection rate and pressure for J-23A. The injection rate stabilized at 1450 barrels per day (bpd) while the wellhead pressure stayed slightly below 1000 psi for the reporting period which is the maximum designed pressure for the injection pumps. The plan is to replace the pumps' plungers to achieve higher injection pressures. To date 350,000 pounds of polymer have been injected into J-23A and the cumulative volume of polymer solution injected is 712,000 barrels representing 7.4%

of the total pore volume of the flood pattern.

Figure 5.2: J-23A injection rate and pressure.

Figure 5.3 presents daily injection rate and pressure for J-24A. The injection rate stabilized at 600 bpd at a wellhead pressure of 850 to 980 psi. Apparently, this well's injectivity increased in mid-November since the wellhead pressure decreased by 80 psi from 930 to 850 psi while the injection rate was kept constant. This phenomenon was most likely caused by sand dilation in the reservoir where the unconsolidated sand moves around as water or polymer solution is injected into the formation. To date 150,000 pounds of polymer have been injected into J-24A and the cumulative volume of polymer solution injected is 310,000 barrels representing 4.9% of the total pore volume of the flood pattern.
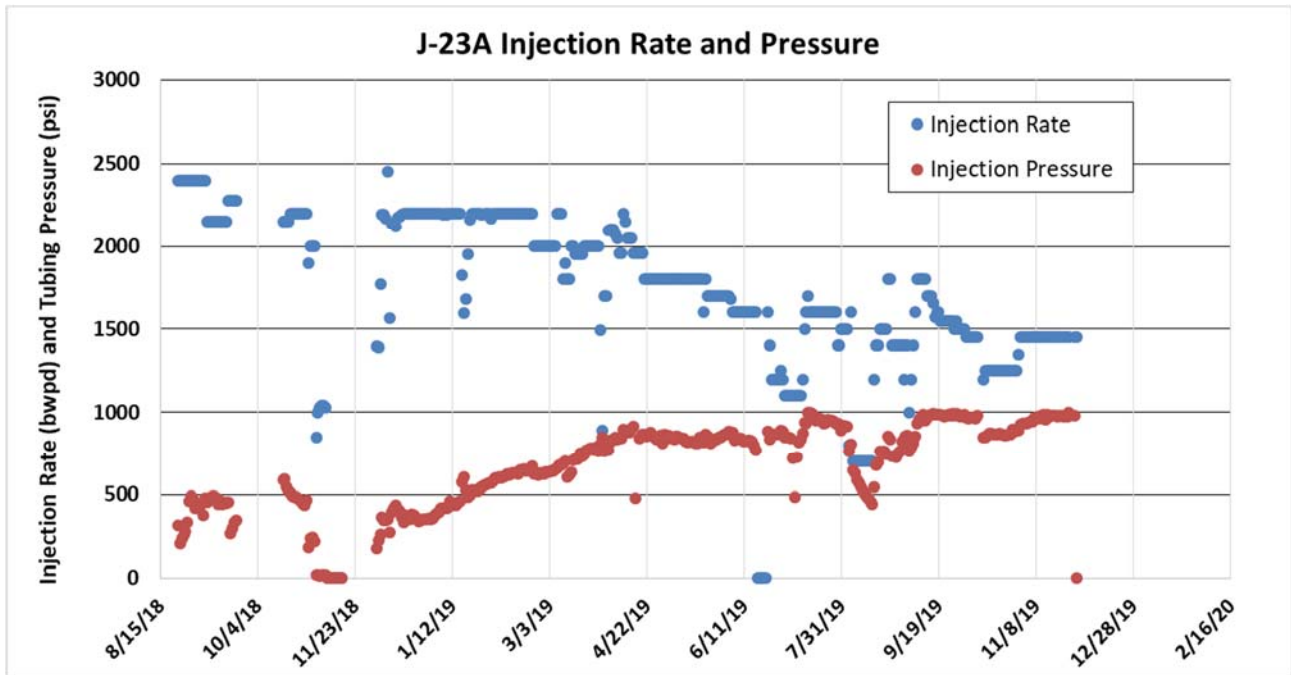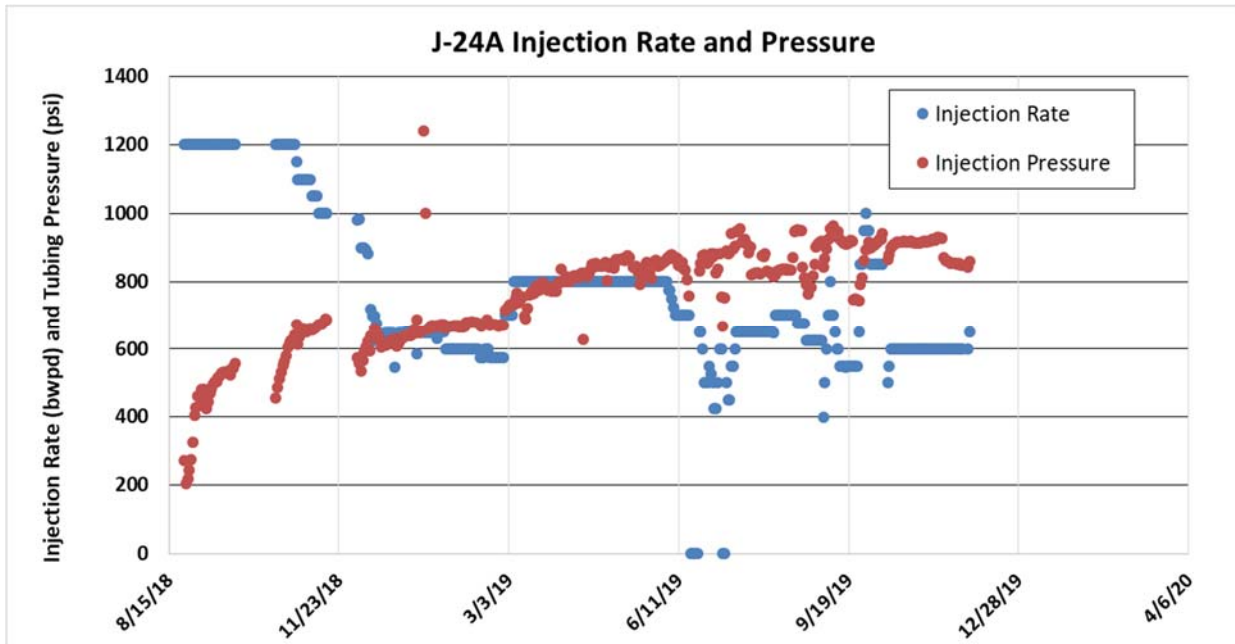
Figure 5.3: J-24A injection rate and pressure.

Figure 5.4 is a Hall Plot for both J-23A and J-24A, which plots the integration of the differential pressure between the injector and the reservoir versus cumulative water injection. The data would form a straight line if the injectivity stays constant over time, curve up if the injectivity decreases and vice versa. After a decrease in the injectivity earlier, current Hall plot diagnostic indicates that the injectivity of both J-23A and J-24A have stabilized.

Figure 5.4: Hall plot for J-23A and J-24A.

Voidage Replacement Ratio
Figure 5.5 presents the instantaneous (blue circles) and cumulative (red line) voidage replacement ratios

(VRR) of the project patterns. VRR is defined as the ratio of the injection volume to production volume at reservoir conditions. During the first 4 months of polymer injection from August to December 2018, instantaneous VRR<1 meaning that the polymer injection volume was less than the production voidage. However, since January 2019, instantaneous VRR>1 meaning that the polymer injection volume was greater than the production voidage due to the decline in total liquid (oil + water) production rate.
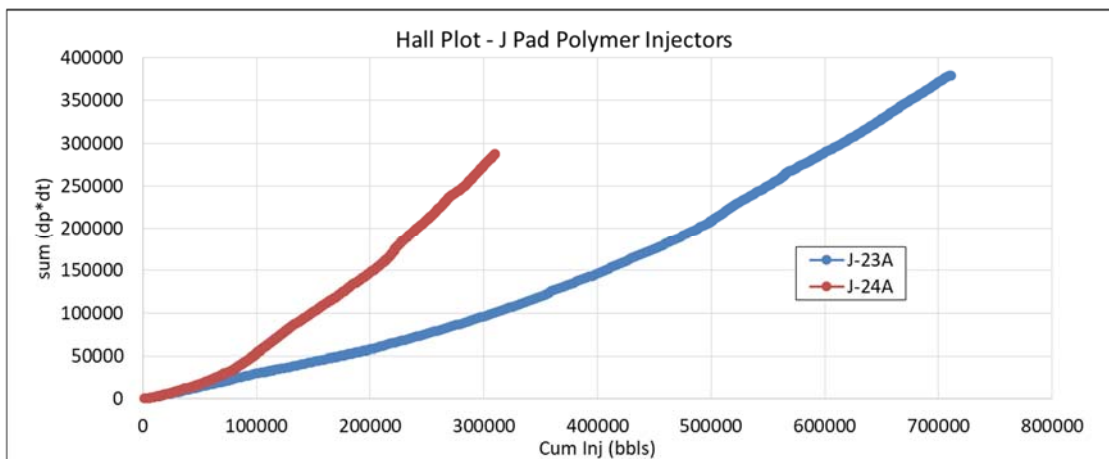
Cumulative VRR of the project pattern was 0.85 at the beginning of polymer injection and currently at approximately 0.86 meaning that we have injected slightly more polymer solution than the production voidage during the last 15 months. Note that this is the delta VRR of 0.01, which is relative over WF. In order to increase oil production rate, current plan is to continue over inject to catch up with the voidage replacement to increase the reservoir pressure to its initial value.
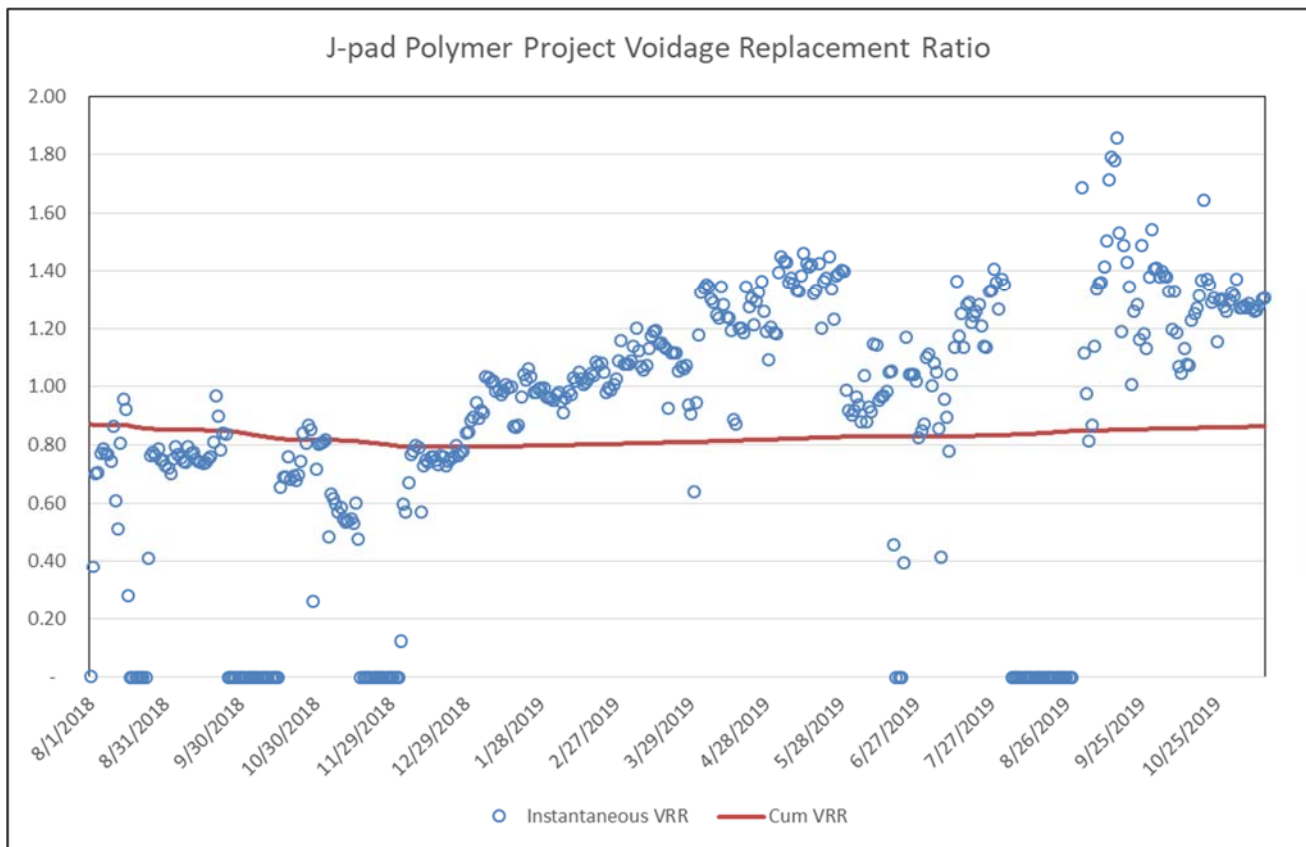

Figure 5.5: Voidage replacement ratio

Production Performance

Figure 5.6 depicts the production performance of producer J-27 which is supported by both injectors, J-23A from the south side and J-24A from the North. Since the start of polymer injection, water-cut has decreased from 67% to 30% which is the best indicator that the injected polymer is helping improve sweep efficiency. Total liquid rate has also been declining due to several factors: (1) Decrease in reservoir pressure due to low voidage replacement ratio (cum VRR<1); (2) Blocking of high permeability channel by polymer; and (3) higher bottom-hole flowing pressure due to the ailing ESP.
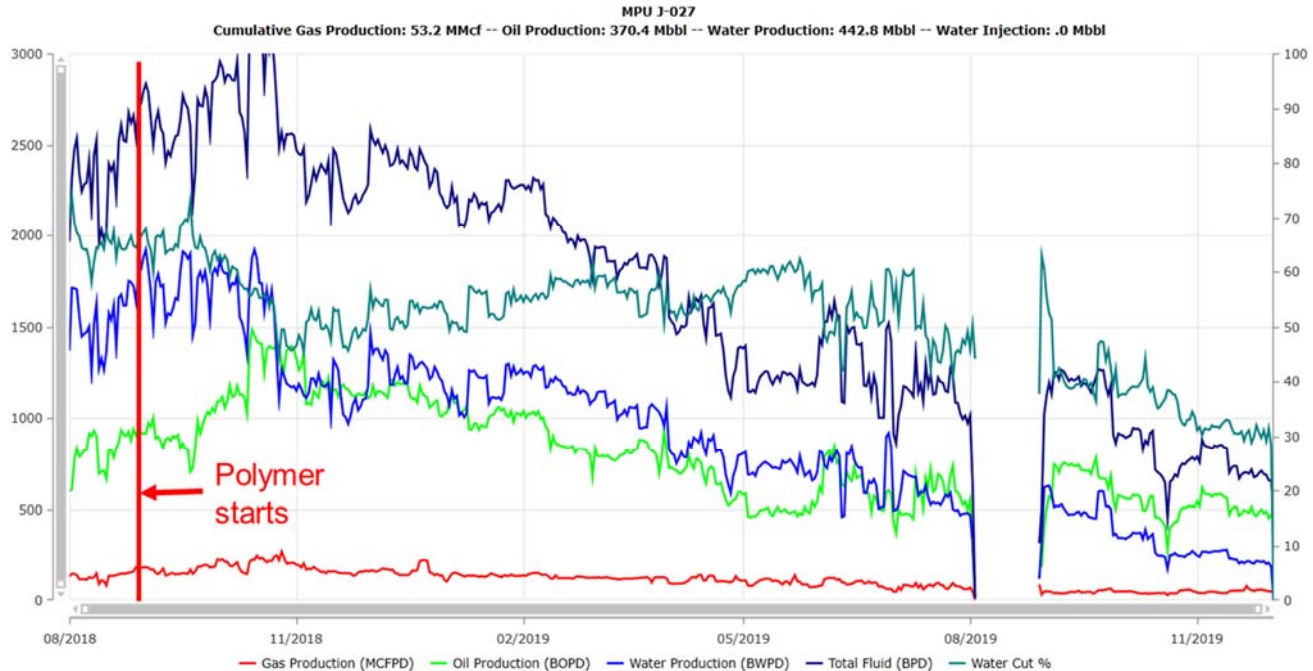
Figure 5.6: J-27 production performance.

Figure 5.7 depicts the production performance of producer J-28 which is supported only by J-23A from the north since the south side is adjacent to a sealing fault. Water-cut has decreased from 70% to 20% since the start of polymer injection. The fast response in water-cut is most likely caused by polymer blocking off the high permeability channels which were probably responsible for the fast increase in water-cut before polymer injection started. Oil rate has increased to ~700 bpd from ~500 bpd before polymer injection. Had polymer injection never started, the oil rate would have been much lower than 500 bpd due to the fast increase in expected water-cut when water-flooding a heavy oil reservoir.
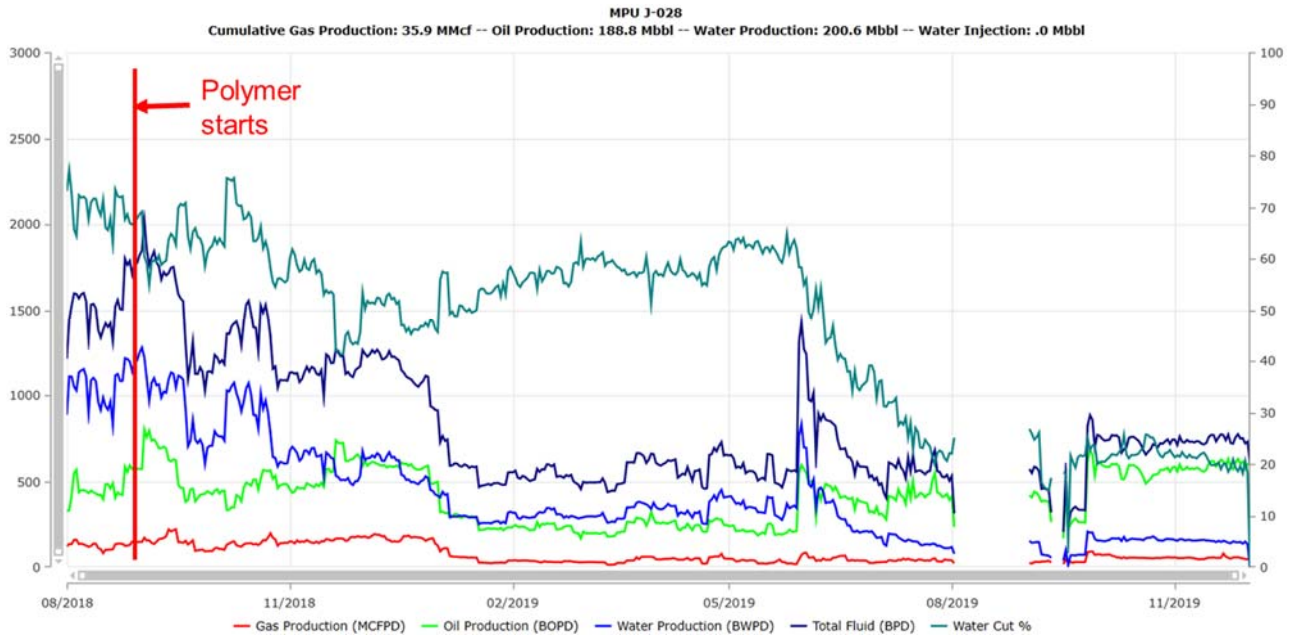
Figure 5.7: J-28 production performance.

Estimated Incremental Oil Rate

A reservoir simulation model has been developed and history-matched to predict the incremental oil benefit from polymer flood versus waterflood. **Figure 5.8** shows the total predicted oil rate under waterflood (blue line) and polymer flood (magenta line) processes from the 2 project wells. The difference between the two represents EOR benefit which is estimated to be approximately 600 bpd at the present time.
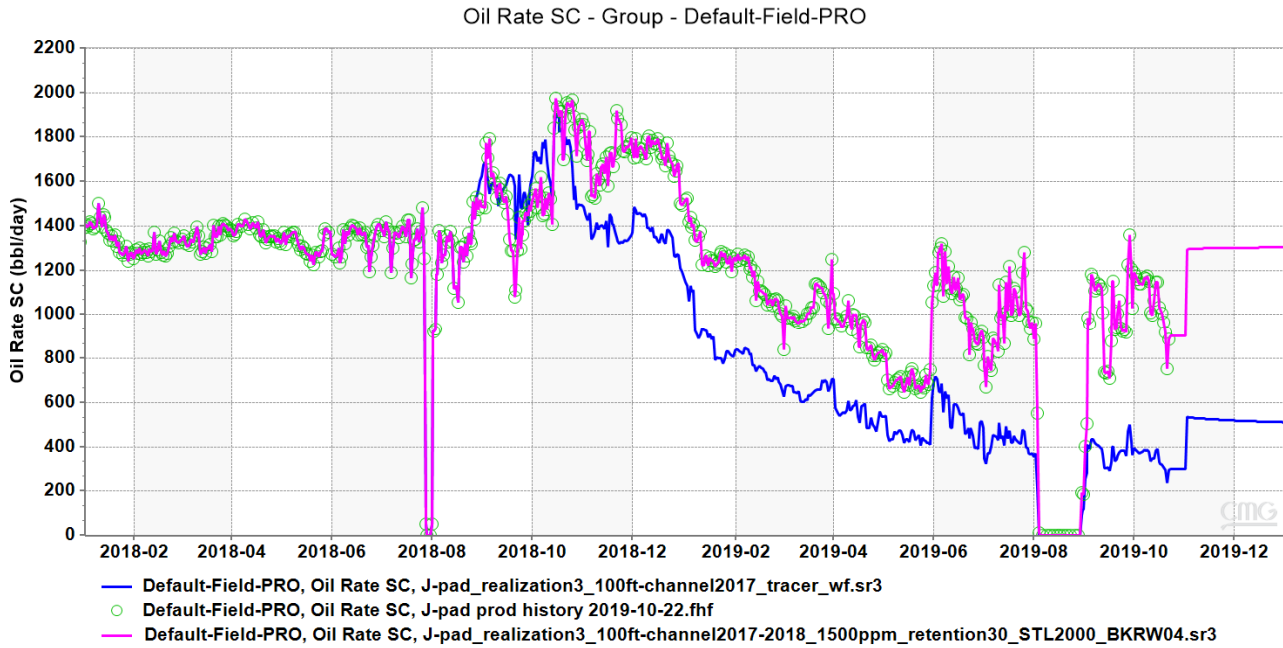
Figure 5.8: Predicted total oil rate under waterflood and polymer flood processes.

Pre-Polymer Tracer Test

Two different tracers named T-140C and T-140A were pumped into injectors J-23A and J-24A respectively on August 3, 2018, 25 days prior to the start of polymer injection. Produced water samples are taken weekly from producers J-27 and J-28 and analyzed to detect tracer concentration. The latest produced tracer concentration is shown in **Figure 5.9**. The time of appearance (breakthrough) and the magnitude of the tracer concentration in the two producers are indicators of injector-producer communication and the volumetric sweep efficiency in the flood pattern.
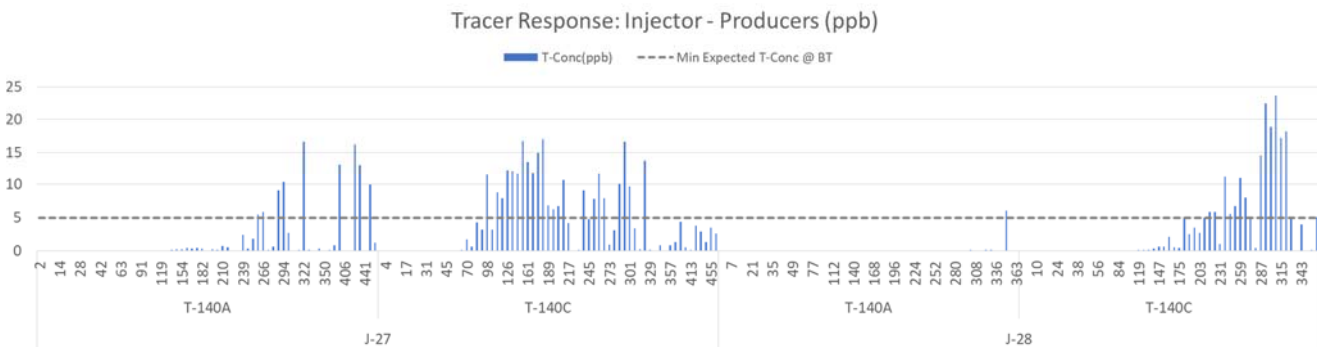
Figure 5.9: Tracer concentration in produced water.

Tracer T-140C from J-23A first appeared in producer J-27 after 70 days of injection indicating strong communication between the well pair. However, the fast breakthrough timing also indicates that the sweep efficiency of water displacing oil is low. Assuming no more tracer will be produced from now on,

the volumetric sweep efficiency from waterflood was estimated to be less than 3% in the particular reservoir sector between injector J-23A and producer J-27.

Tracer T-140C from J-23A first appeared in producer J-28 after 140 days of injection indicating that communication between the well pair is slower which also means that the injected water was sweeping more oil before being produced out of the reservoir. Estimated volumetric sweep efficiency from waterflood was approximately 9%, assuming no more tracer will be produced from now on.

Tracer T-140A from J-24A also first appeared in producer J-27 after 140 days of injection. The communication in this well pair is slower than from J-23A to J-27. Estimated volumetric sweep efficiency from waterflood was also less than 3%, assuming no more tracer will be produced from now on. It is important to note that the low sweep efficiency by waterflood creates a great opportunity for polymer flood.

Post-Polymer Tracer Test
Five months after polymer injection started, two more tracers, T-803 and T-801, were pumped into injectors J-23A and J-24A respectively to monitor polymer breakthrough timing and estimate sweep efficiency for polymer displacing oil. To date, 8 months after injection, no significant tracer concentration has yet been detected from the two producers indicating that that all polymer injected so far are still sweeping oil in the reservoir. We will continue sampling the produced water weekly and testing for the tracer and polymer contents to assess the sweep efficiency of polymer displacing oil.

Monitoring Polymer Breakthrough
Since the start of polymer injection, produced water samples have been collected weekly and analyzed onsite using the clay flocculation test, as well as in the laboratory via nitrogen-fluorescence water composition analyses to detect the presence of produced polymer in the production stream. As of the end of November 2019, 15 months after the start of polymer injection, no polymer has been observed in the production stream.

Main Observations from Field Pilot to Date
1. Adequate polymer injectivity can be achieved with horizontal wells in the Schrader Bluff N-sand reservoir. But polymer solution quality control is critical to ensure polymer propagation through the reservoir.
2. Water cut has decreased from 67% to approximately 24% in the project wells since the start of polymer injection. Estimated EOR benefit is approximately 600 bopd at the present time.
3. Fifteen months after the start of polymer injection, no polymer production has been confirmed from the producers yet compared with waterflood breakthrough timing of 3 months. Furthermore, no post polymer tracer production has been detected either, 8 months after tracer injection.
4. The drastic decrease in water cut and delayed polymer breakthrough both indicate significant improvement in oil sweep by the injected polymer.
5. More polymer injection is needed to calibrate the reservoir simulation models and accurately quantify the EOR benefit.

Activity is ongoing.

● Task 6.0 -Analysis of Effective Ways to Treat Produced Water that Contains Polymer

Experimental details
In the reporting quarter, oil water separation studies have continued for synthetic emulsions at 20% and 75% water cut (WC) prepared in the lab. The detailed bottle test procedures have been described in previous report, thus they are not repeated here. To be noted, the un-sheared polymer solution was used in order to test the worst case condition. To prepare the compound emulsion breaker, two kinds of emulsion breaker are well premixed before addition to the emulsion.

Results and Discussion
The effect of polymer on separation behaviors of synthetic emulsions. Oil-water separation behavior is characterized by water separation kinetics, oil content in the separated water (OIW) and volume fraction of the separated phases respectively. **Figure 6.1** shows the effect of polymer concentration on separation kinetics at 20% and 75% WC. Water separation kinetics can be used to describe the emulsion stability; the faster the water can separate, the less stable the emulsion is. With no addition of polymer, the emulsion generated at 20% WC was much more stable than that at 75% WC. The emulsion at 20% WC was stable for at least 24hrs; however, the emulsion at 75% WC was quite unstable separating into two layers in less than 5mins.

In the presence of polymer, the phase separation was accelerated for emulsions at 20% WC; and the amount of separated water at first increased with increasing polymer concentration and then followed by decrease when the polymer concentration reached the critical point of 400ppm. To be noted, more than 100% of water was separated for 400ppm and 800ppm polymer. This is because the intermediate layer is accounted into the measure of water volume since the interface between the water layer and the intermediate layer cannot be well defined. For emulsion at 75% WC, the presence of polymer significantly impeded the phase separation which is due to the increasing viscosity of polymer solution. To be noted, the separation efficiency in the presence of polymer was slightly above that of the emulsion without polymer. It is due to the massive oil content in the water which could affect the measurement of water volume.
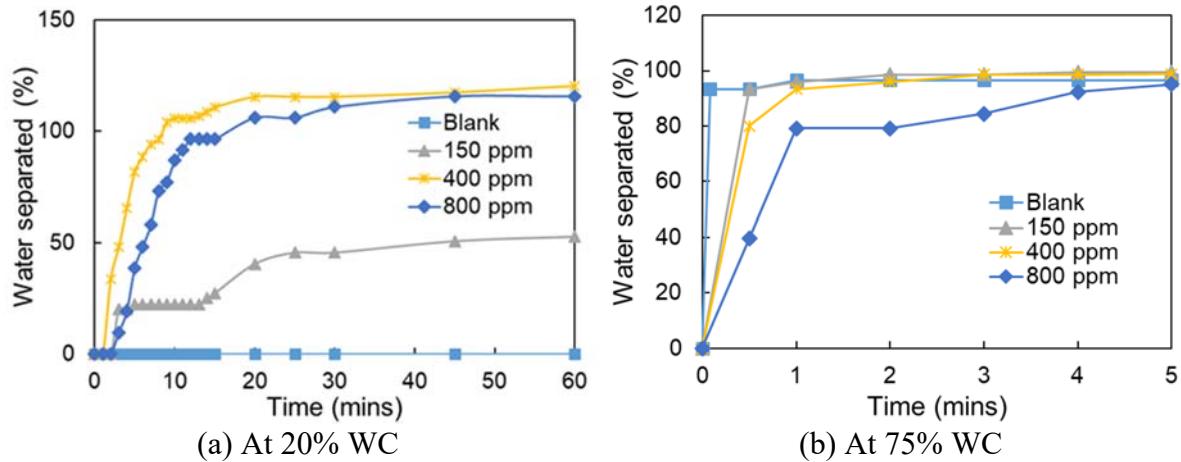
(a) At 20% WC (b) At 75% WC

Figure 6.1: The effect of polymer on separation kinetics

The effect of polymer on the separated water quality after 24hrs is displayed in **Figure 6.2**. The polymer had a negative effect on the separated water quality for emulsions at both 20% WC and 75% WC. The OIW significantly increased with increasing polymer concentration. In the absence of polymer, a small amount of tiny oil droplets were trapped in the separated water and was stable for 24hrs because they have a less possibility to collide due to the low concentration. With addition of polymer, more oil droplets were trapped since polymer can result in smaller drop size and more rigid interfacial film which makes it more difficult for oil droplets to coalesce (Liu et al., 2015). At certain polymer concentration, OIW at 75% WC was two times higher than that at 20% WC which implies the water treatment is much more challenging at high WC.

(a) At 20% WC (b) At 75% WC
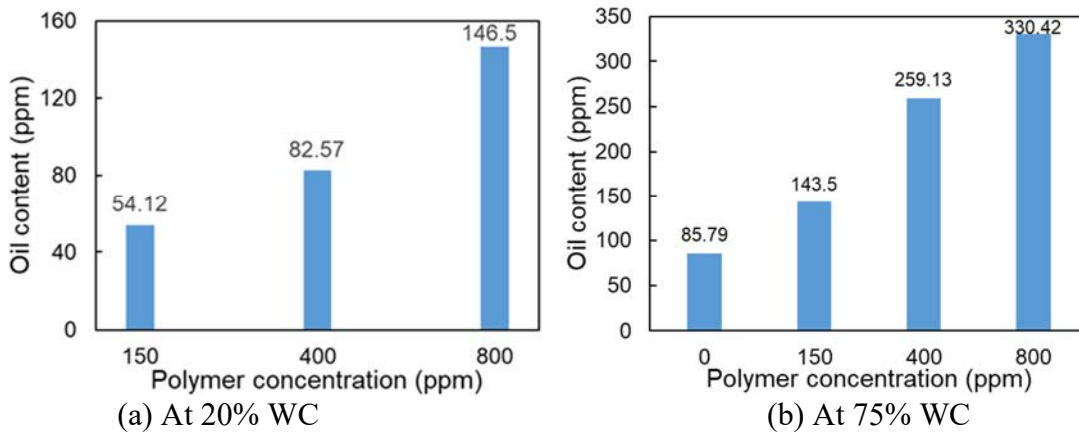
Figure 6.2: The effect of polymer on water quality

It is worth mentioning that a residue concentrated o/w emulsion layer is even noticed between the top oil layer (w/o emulsion) and the bottom dirty water layer as shown in **Figure 6.3**. The interfaces between this intermediate layer and the top layer or bottom layer became clearer as the settling time prolonged. After 24hrs, this intermediate emulsion layer still persisted. The thickness of this layer had a relationship

with the water cut. The lower the water cut, the thicker the intermediate layer. The thickness of this layer with respect to time also depended on the water cut. The intermediate layer became thinner with time at 20% WC but thicker at 75% WC. The formation of the residue emulsion in the middle is certainly due to the higher viscosity of the aqueous phase that hinders the oil-water separation.

(a) At 20% WC   (b) At 75% WC

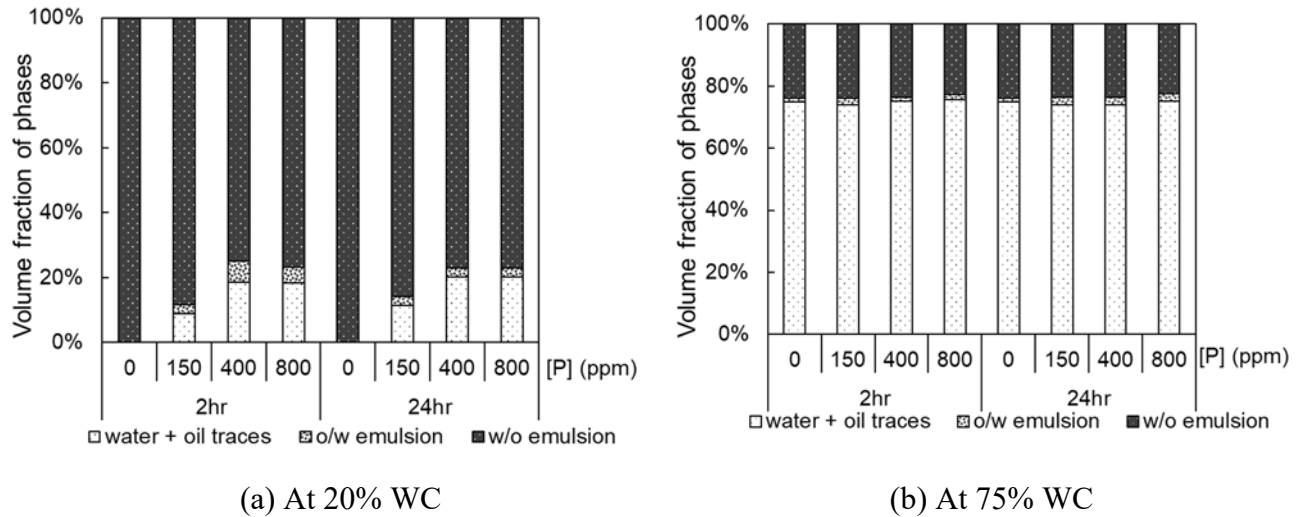**Figure 6.3: The effect of polymer on the volume fraction of phases**

Emulsion breaker performance for synthetic emulsions without polymer. The performance of individual emulsion breakers and one compound emulsion breaker which performs best at 50% WC is investigated by bottle test method.

Performance of different emulsion breakers. The performance of demulsifiers with a dosage of 100ppm for emulsions without polymer at 20% WC is shown in **Figure 6.4**. It is found all four oil-soluble emulsion breakers accelerated the phase separation and obtained clear water phase with OIW lower than 50ppm. Among all four emulsion breakers, E12+E18 and E18276A yielded similar separation efficiency and OIW, implying E12+E18 can be a substitute for E18276A when applied to emulsion at 20% WC. However, water-soluble emulsion breaker N1691 exhibited no water separation. The poor performance of N1691 can be explained by its weak solubility in w/o emulsion which caused the barriers to the diffusion and adsorption process of N1691 molecules (Kang et al. 2018). To be noted, even though E18276A and E12+E18 had the best performance, they did not render complete separation of the water phase in the measured time scale.
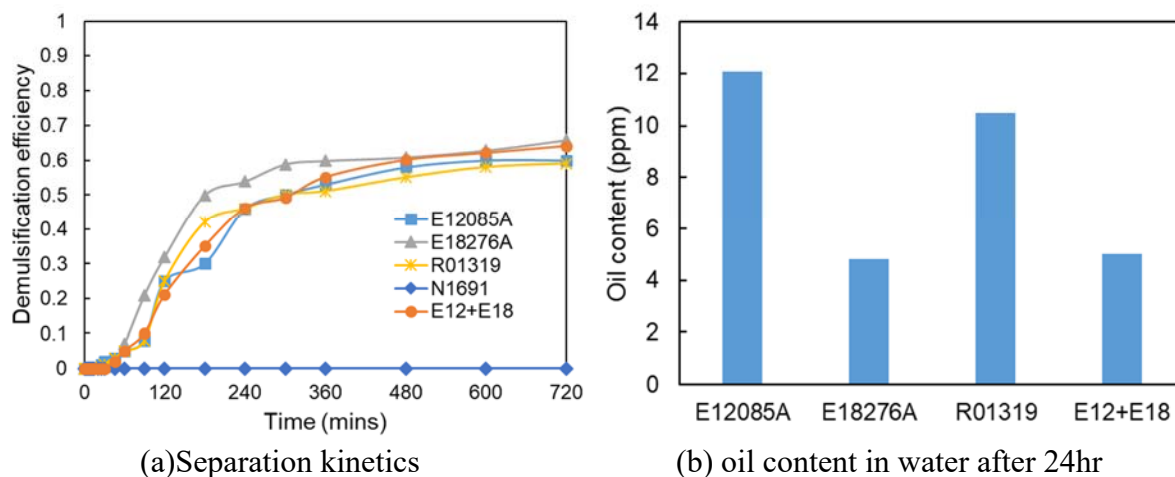
(a)Separation kinetics   (b) oil content in water after 24hr

Figure 6.4: The performance of demulsifiers for emulsions without polymer at 20% WC

The performance of demulsifiers at a dosage of 100ppm for emulsion at 75% WC is shown in **Figure 6.5**. All tested emulsion breakers had a good performance with separation efficiency more than 90% and OIW lower than 50ppm. E12+E18 showed a slight advantage over other emulsion breakers in terms of separation efficiency.

(a) Separation kinetics   (b) oil content in water after 24hr
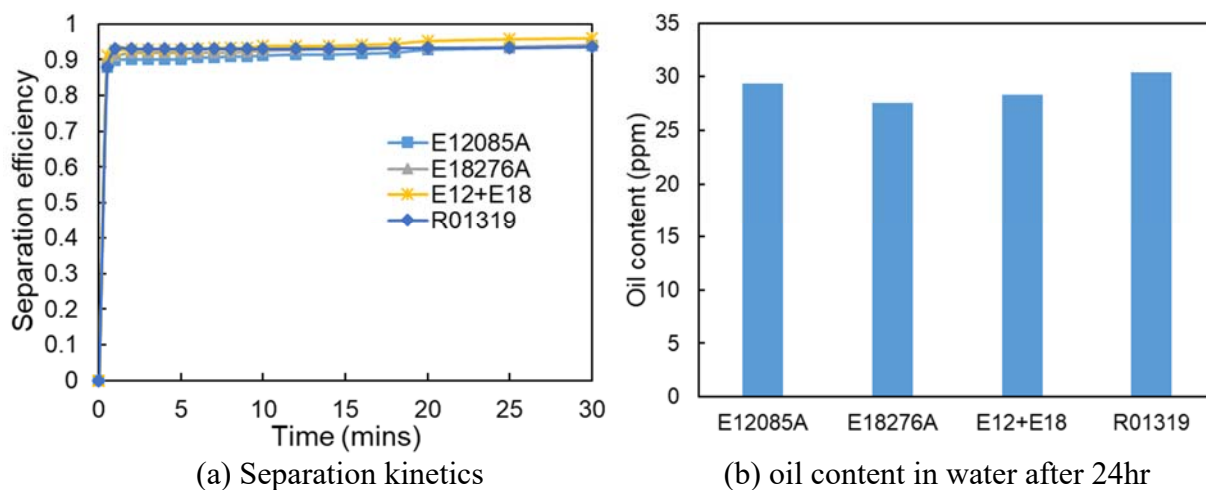
Figure 6.5: The performance of demulsifiers for emulsions without polymer at 75% WC

Performance of emulsion breaker at different dosage rate. Increasing the emulsion breaker dosage is one typical way to improve the phase separation and the optimized dosage is of great importance for the field application due to the side effects of over-dosage, such as decreased separation efficiency, poor water quality, massive oil adhesion and so on. As mentioned before, E18276A did not yield a separation efficiency of over 90% at the dosage of 100ppm. To improve the separation, the demulsifier dosage was increased and the results are shown in **Figure 6.6**. A remarkable increase of the separation efficiency and OIW was observed with increasing dosage. The OIW was beyond the discharge standard when the dosage

University of Alaska Fairbanks

was above 300ppm.
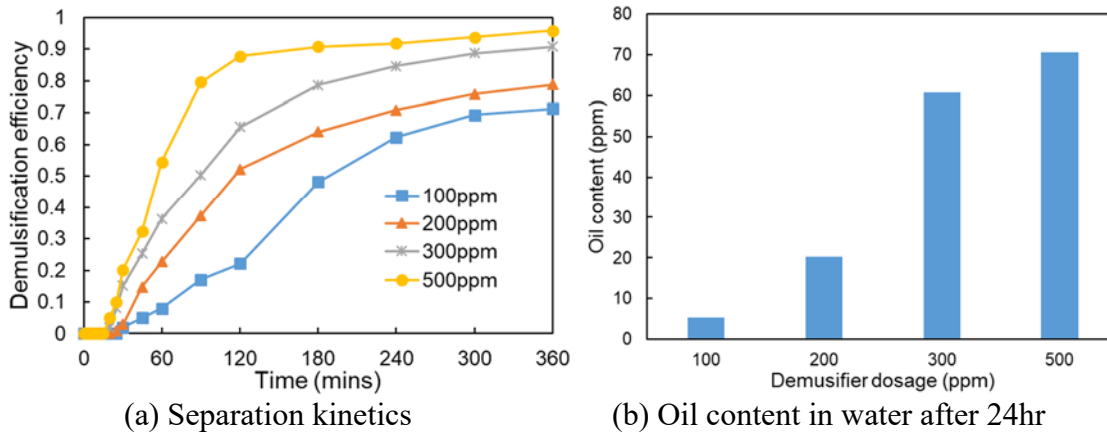
(a) Separation kinetics   (b) Oil content in water after 24hr
Figure 6.6: The effect of dosage on the performance of E18276A

Emulsion breaker performance for synthetic emulsion with polymer. Emulsion breaker should counteract the negative effects brought by the addition of polymer, such as the reduced separation speed, the formation of intermediate layer and the poor quality of separated water. The performance of multiple emulsion breakers is evaluated to select the best emulsion breaker for emulsions with polymer.

Performance of different emulsion breakers. The performance of emulsion breakers at a dosage of 100ppm for the emulsion with 150ppm polymer, which is the most stable emulsion at 20% WC, is shown in **Figure 6.7**. According to the results, all four oil-soluble demulsifiers can effectively eliminate the intermediate layer and obtain a clear water phase. Note that the separation efficiency of four oil-soluble emulsion breakers in the order from highest to lowest is E18276A > E12+E18 > E12085A > R01319. Based on the analysis, E18276A and E12+E18 are highly competent for emulsions with 150ppm polymer at 20% WC.

The performance of emulsion breakers at the dosage of 10ppm for the emulsion with 800ppm polymer, which is the most stable emulsion at 75% WC, is shown in **Figure 6.8**. All tested emulsion breakers had similar performance. E12+E18 showed a slight advantage over other emulsion breakers in terms of separation speed and OIW. To be noted, all the emulsion breakers except E12+E18 yielded OIW of more than 50ppm, bringing a potential challenge to the produced water treatment.
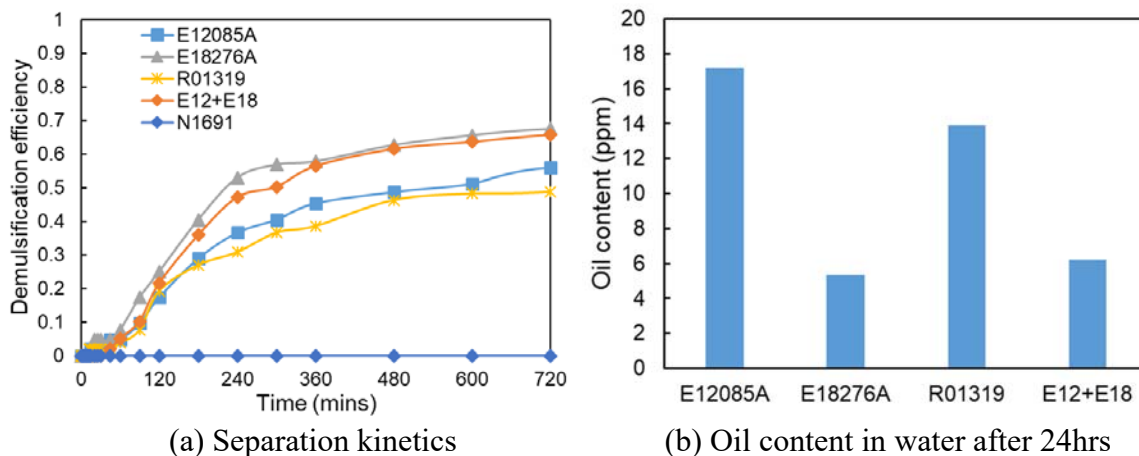
(a) Separation kinetics   (b) Oil content in water after 24hrs

Figure 6.7: The performance of emulsion breakers for emulsion with 150ppm polymer at 20% WC

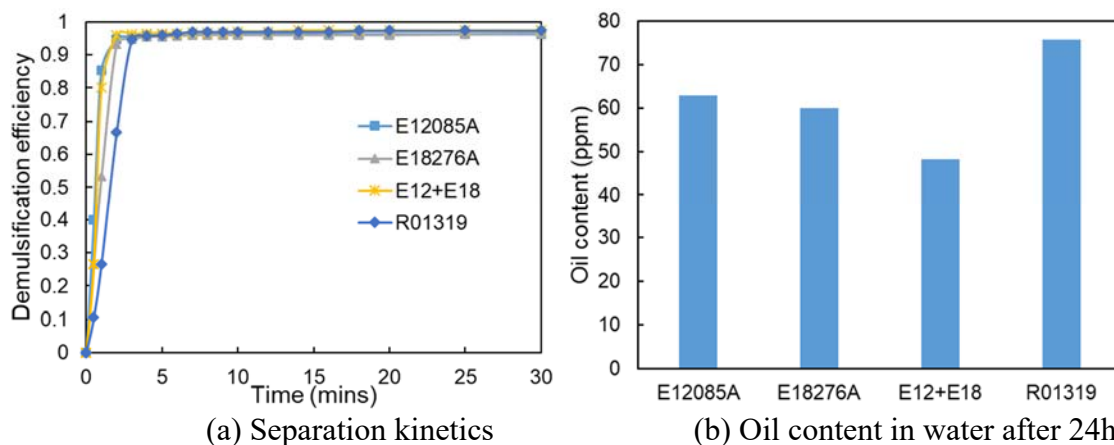(a) Separation kinetics   (b) Oil content in water after 24hrs

Figure 6.8: The performance of emulsion breakers for emulsion with 800ppm polymer at 75% WC

The effect of dosage on emulsion breaker performance. Due to the slightly weak performance of E12+E18 comparing with E18276A at low dosage when treating the emulsion at 20%WC, the performance of E12+E18 is evaluated at different dosage to further validate the applicability of E12+E18, as shown in **Figure 6.9**. In spite of the weak performance of E12+E18 at low dosage of 100ppm, E12+E18 yielded a slightly higher separation efficiency and lower OIW than E18276A when the dosage is above 100ppm, implying E12+E18 can be actually treated as a substitute for E18276A.

For emulsion with 800ppm polymer at 75% WC, the increasing EB dosage is unfavorable for oil-water separation, leading to a reduction of demulsification efficiency as shown in **Figure 6.10**. Besides, at high EB dosage, the oil separated sitting on the top existed in the form of droplets especially at oil-water interface. It could be because the excessive emulsion breaker molecules act as emulsifier at the oil-water interface, preventing the coalescence of oil droplets. In this case, a low dosage of 10ppm is preferable to

prevent the counterproductive effect of over-dosage. Based on the above analysis, compound emulsion breaker E12+E18 has the potential to be used for emulsion at both 20% WC and 75% WC but at different dosage.
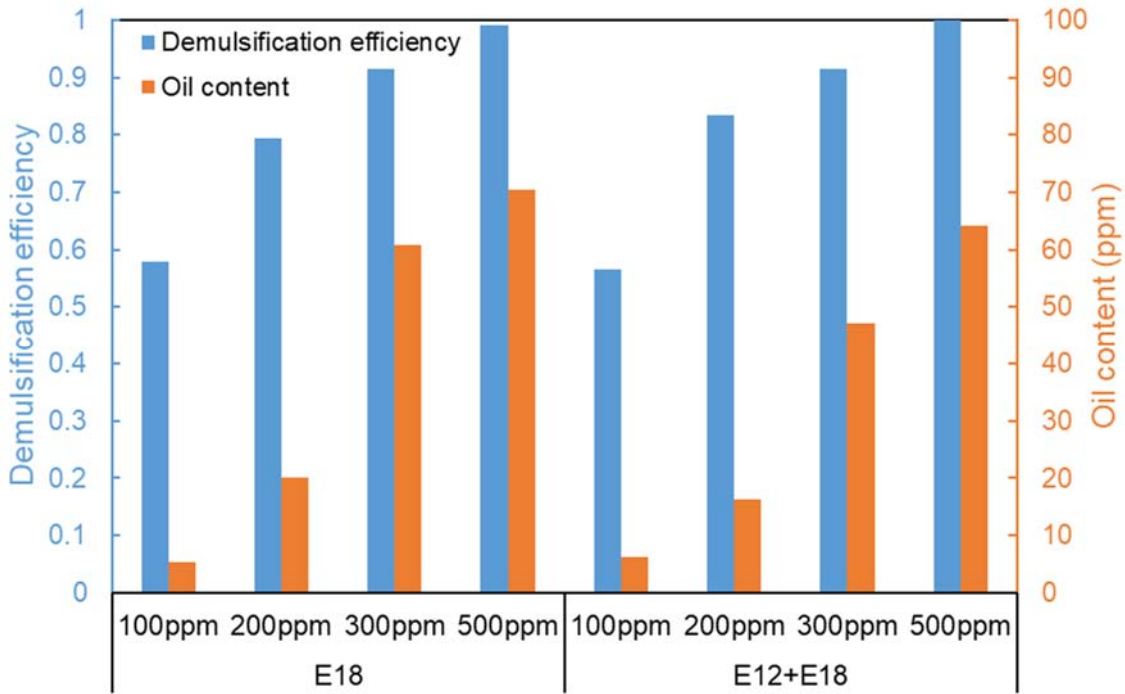

Figure 6.9: The effect of dosage on emulsion breaker performance for emulsion with 150ppm polymer at 20% WC
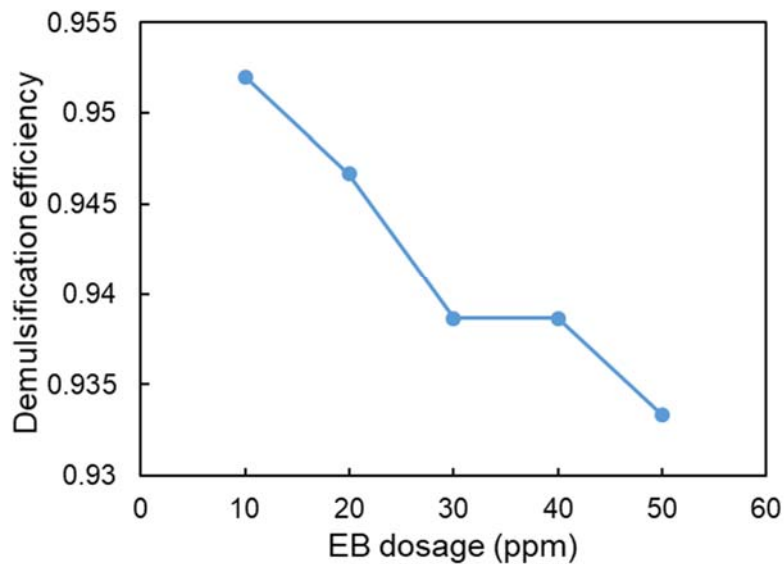

Figure 6.10: The effect of dosage on emulsion breaker performance for emulsion with 800ppm polymer at 75% WC

Future Work
This will focus on studying the effect of salinity and clay particles on the separation behavior of emulsions and the performance of emulsion breakers.

● Task 6.0a –Polymer Fouling of Heater Tubes

Experimental Details
In the reporting quarter, fouling experiments were continued on copper tubes and carbon steel tubes. For copper tubes experiments were done at 165^oF, 200^oF, 250^oF and 350^oF tube skin temperatures. For carbon steel tests were done at $165\,^o$F skin temperatures. For copper tubes two more polymer concentrations were analyzed, namely 80ppm and 600ppm. The procedure for experiments was same as reported in previous quarter. X-Ray Diffraction (XRD) analysis was carried out on deposit generated on tube surface with and without polymer solutions. Deposit rate was defined as a parameter indicating the degree of fouling on tubes for all the results.

$$Deposit\ Rate = \frac{Cumulative\ Deposit\ in\ 5\ Runs\ (mg)}{Total\ Time\ to\ heat\ Testing\ Solutions\ in\ 5\ Runs\ (minutes)} \qquad (6.1)$$

Results and Discussion
The effect of polymer concentration and temperature. Deposit rate increased for increasing polymer concentrations at all temperatures for copper tubes. For temperature points of 165^oF and 200^oF the amount of fouling seen was much less as compared to 250^oF and 350^oF and it is believed these could be safer temperatures to operate the heaters. The two new concentrations – 0ppm and 600ppm have followed the trends of previous results. The deposit rates for copper at all tested polymer concentrations and temperatures are shown in the **Figure 6.11.**
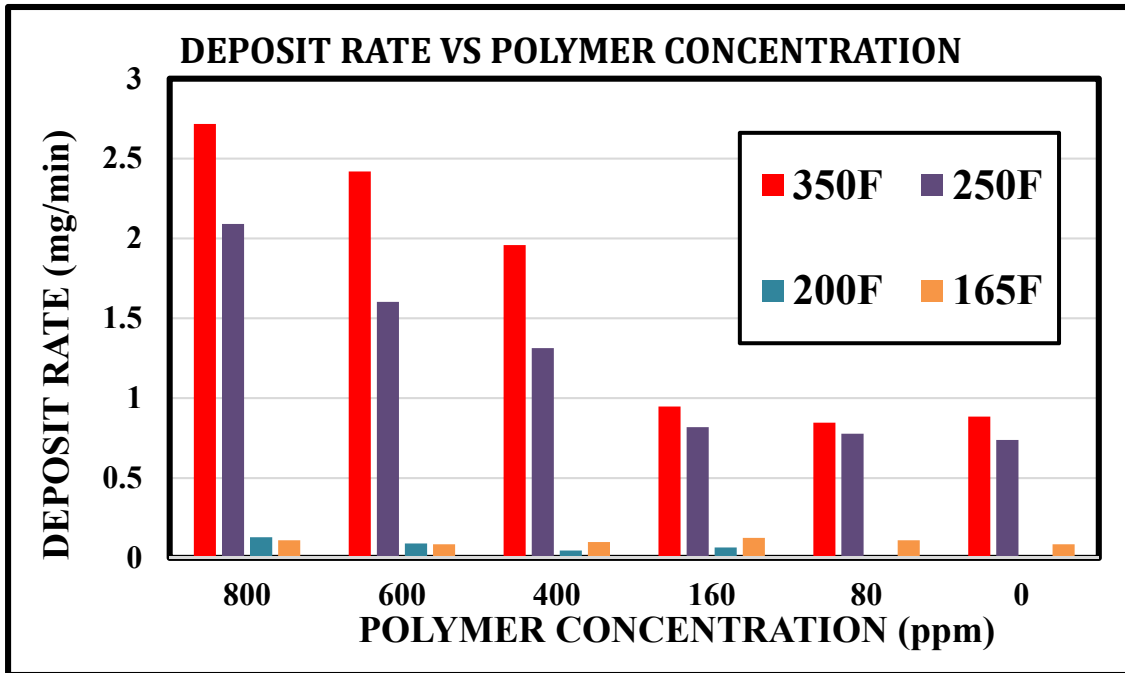
Figure 6.11: Deposit rate comparison at different temperatures and polymer concentrations

Effect of Tube Material – Carbon Steel. Carbon Steel was tested at 165°F at two polymer concentrations – 0ppm and 800ppm. The deposit rates for carbon steel are shown in the **Figure 6.12** below.
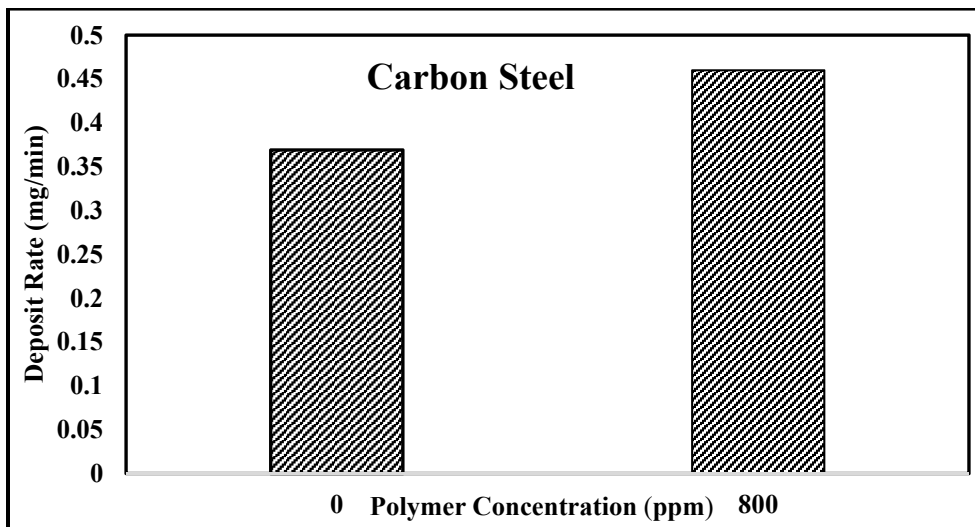
Figure 6.12: Deposit rate for carbon steel

The deposit rate for both with and without polymer scenarios for carbon steel was higher than copper and stainless steel and the tube was also oxidized to a higher extent in the presence of polymer.

X-Ray Diffraction (XRD). The results for XRD of deposit generated on copper tube surface at 350°F at two concentrations – 0ppm and 800ppm are shown in **Figure 6.13.** The compositional analysis done by HighScore Plus software are shown in **Figure 6.14.**

Figure 6.13: X-Ray diffraction patterns of deposit generated by 0 ppm polymer solution and 800 ppm polymer solution at 350°F tube skin temperatures

(a)   Sample without Polymer   (b) Sample with Polymer
Figure 6.14: Compositional analysis of deposit generated using HighScore plus software

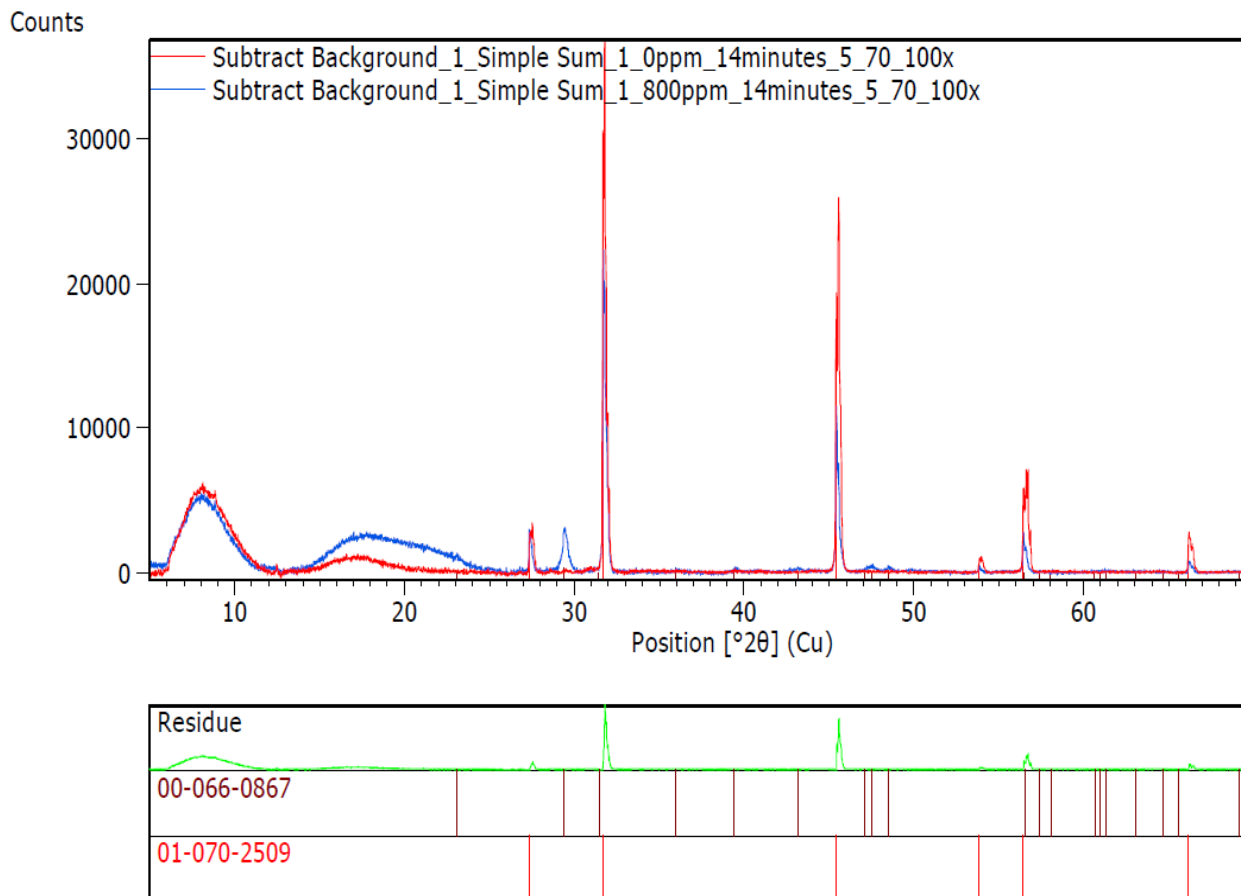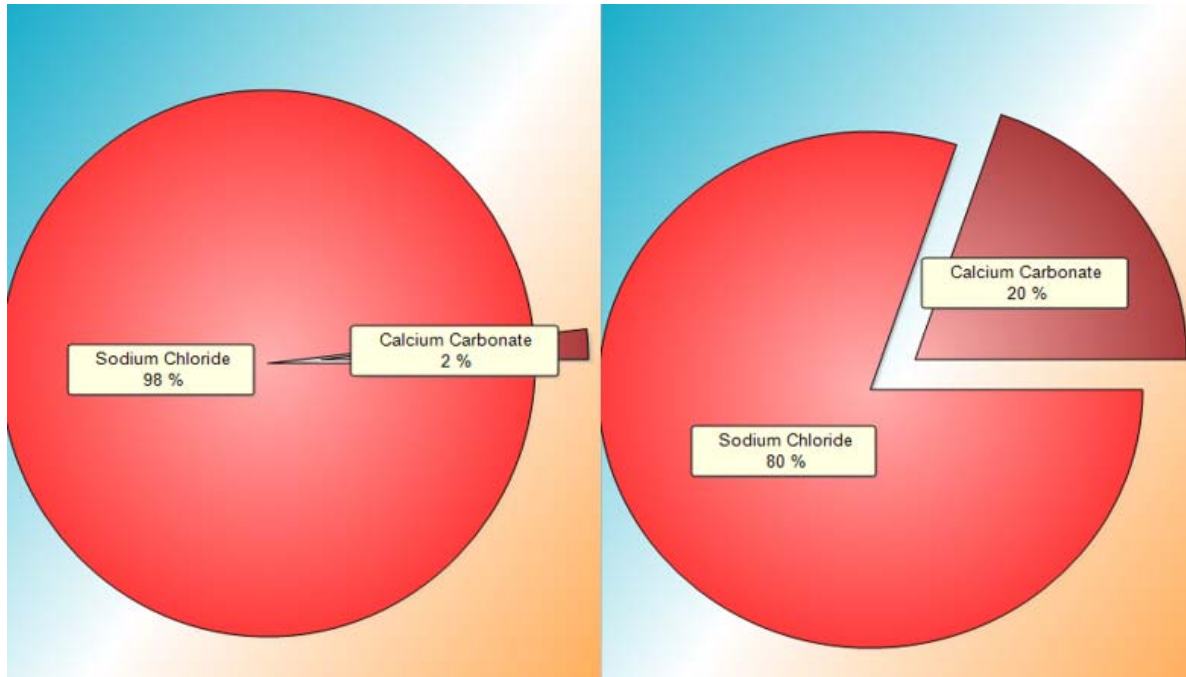The compound codes given below the pattern (**Figure 6.13**) represent sodium chloride - Halite (01-070-2509) and calcium carbonate - Calcite (00-066-0867). With the presence of polymer an additional peak of Calcite was seen in XRD at $2\theta = 29$. Additionally, background noise is observed between $2\theta = 15$ to $2\theta = 24$ in the case of polymer deposit sample. The composition of deposit also changed as it can be seen in the **Figure 6.14** as the amount of calcite increased from 2% without polymer to 20% when polymer is present.

Future Work
Copper tubes at 200ºF for 80ppm and 600ppm polymer concentrations will be tested. A cloud point determination experiment will also be carried out to see hydrolyzed polyacrylamide stability at different concentrations. Dynamic scale loop has been setup and results will be reported in the next quarter.

Both activities are ongoing.

● Task 7.0 - Feasibility of Commercial Application of the Proposed Advanced Polymer Flooding in ANS Heavy Oil Reservoirs

Activity has not yet started, since it is scheduled for BP4.

 c.   **Opportunities for Training and Professional Development**
All the graduate students working on the project are obvious recipients of training and professional

development in petroleum engineering. First authors of two of the accepted papers for the 2020 SPE-IOR meeting are UAF MS (Anshul Dhaliwal) and PhD (Hongli Chang) students that are supported by the project, who will present the respective papers at the conference, which will obviously provide them excellent professional development opportunities. Finally, the project team Thanks Hilcorp Alaska LLC for funding Hongli's site visit to Milne Point, where she spent two days learning about the polymer operations and emulsion testing.

d.   Dissemination of Results to Communities of Interest
Engineers from ConocoPhillips and Hilcorp continue to communicate about the project on a regular basis. Additionally, most of the project related information is publically available or disseminated through the NETL website, which is accessible to any communities that have interest in the project. Similarly, publications resulting from the project work also serve the same purpose.

e.   Plan for Next Quarter
Building on the current progress achieved by the research team, work planned for the next quarter will include steadily progressing toward the planned completion dates outlined in **Table A** below.

Table A: Summary of milestone status.

Milestones	Task No.	Planned Completion Date	Actual Completion Date	Verification Method	Comments
Project Management Plan	1a	o 9/30/2022	o Ongoing (latest revision 4/30/2019)	Report/Bi-weekly meetings	None
Data Management Plan	1b	o 8/31/2018	o 7/20/2018 (latest revision 4/30/2019)	Report/Bi-weekly meetings	None
● Quantify polymer retention	2	o 3/31/2019	o Several tests completed but continues to be a topic of investigation	Report/Bi-weekly meetings	None
● Effect of water salinity on S_{or}	3	o 4/30/2019	o Several tests completed per the planned date; however, August 16th marks the true completion.	Report/Bi-weekly meetings	None

● Screening of gel products for conformance control		o 6/30/2019	o Some preliminary tests completed, and continues to be a topic of investigation		
● Pilot area model waterflooding history match	4	o 12/312018	o 2/1/2019; various versions prepared, work is ongoing	Report/Bi-weekly meetings	None
● Coreflooding model history match		o 4/30/2019	o Some completed per plan, but is ongoing		
● Updated area model for polymer flood prediction		o 5/31/2019	o Completed but is also ongoing refinement		
● Reservoir modeling report		o 5/31/2019	o Extensively reported in Quarterlies, but a formal report was submitted on July 11, 2019 as special status report		
● Injection profile with polymer inj. ● PFO (post-polymer) ● Tracer tests (post-polymer)	5	o 12/31/2018 o 12/31/2018 o 12/31/2018	o Ongoing o Ongoing o Ongoing *Note – all have been completed from the reporting standpoint, but given the dynamic nature of the pilot these are also ongoing*	Report/Bi-weekly meetings	None

● Initial treatment plan recommendation based upon literature survey	6	o 12/31/2018	o Ongoing refinement and additional tests. However, recent tests have been used to identify/screen an effective emulsion breaker.	Report/Bi-weekly meetings	None
● Static polymer deposition quantification and analyses		o 09/30/2019	o Tests on copper and carbon steel already completed and the deposit imaged; mostly complete in this quarter		
● Finalization of the fouling flow loop design		o 06/30/2019	o Completed, mostly in this quarter, coils have been prepared for testing		

2. PRODUCTS

Following are the complete citations of the three accepted abstracts for the 2020 SPE-IOR and 2020 SPE WRM conferences respectively. Eventually, these will be cataloged in www.onepetro.org, SPE's online library.

(1) Abhijit Dandekar, Baojun Bai, John Barnes, Dave Cercone, Jared Ciferno, Reid Edwards, Samson Ning, Walbert Schulpen, Randy Seright, Brent Sheets, Dongmei Wang and Yin Zhang: First Ever Polymer Flood Field Pilot to Enhance the Recovery of Heavy Oils on Alaska's North Slope - Pushing Ahead One Year Later, SPE Western Regional Meeting, April 27-30, 2020, Bakersfield, California, USA.

(2) A. Dhaliwal, Y. Zhang, A.Y. Dandekar, S. Ning, J.A. Barnes, R. Edwards, W. Schulpen, D.P. Cercone, J. Ciferno: Experimental Investigation of Polymer Induced Fouling of Heater Tubes in The First Ever Polymer Flood Pilot On Alaska North Slope, SPE-200369-MS, SPE Improved Oil Recovery Conference, SPE-200463-MS, 18 - 22 April 2020, Tulsa, Oklahoma, USA.

(3) H. Chang, Y. Zhang, A.Y. Dandekar, S. Ning, J.A. Barnes, R. Edwards, W. Schulpen, D.P. Cercone, J. Ciferno: Experimental Investigation On Separation Behavior Of Heavy Oil Emulsion For Polymer Flooding On Alaska North Slope, SPE-200369-MS, SPE Improved Oil Recovery Conference, 18 - 22 April 2020, Tulsa, Oklahoma, USA.

(4) D. Wang, C. Li, R.S. Seright: Polymer Retention Evaluation In A Heavy Oil Sand For A Polymer Flooding Application On Alaska's North Slope, SPE-200428-MS, SPE Improved Oil Recovery Conference, 18 - 22 April 2020, Tulsa, Oklahoma, USA.

3. PARTICIPANTS & OTHER COLLABORATING ORGANIZATIONS

Hilcorp hired two operators dedicated to the project operations. Two reservoir engineers are in charge of the test design and analysis; one facilities engineer is in charge of polymer skid design and installation; and one operations engineer is in charge of downhole well work.

All the listed project personnel identified on the second page, and graduate students working on different tasks formally contribute 2 hours every other Friday in a project working meeting. Additionally, sub-group working meetings, typically lasting for 2-4 hours in a month are also held to discuss specific tasks such as reservoir simulation. For graduate students, the typical formal working hours per week are 20. Besides these, additional hours are typical in preparing reports, presentations for meetings, and potential publications.

4. IMPACT

The project continues to be an outreach tool since it is actually showcased (relevant parts of it) in the petroleum engineering curriculum, and is a topic of frequent technical discussions, at many places.

5. CHANGES/PROBLEMS

None to report in this quarter.

6. SPECIAL REPORTING REQUIREMENTS

Nothing to Report.

7. BUDGETARY INFORMATION

A summary of the budgetary information for the first budget period of the project is provided in **Table B**. This table shows the planned costs, reported costs, and the variance between the two. Reported costs is the sum of UAF's incurred expenses and the sum of the invoices received from our project partners.

Table B: Budgetary information for Budget Period 2, Q2.

Baseline Reporting Quarter	Budget Period 2	
	September 1 2019 – November 30 2019	
	Q2	Cumulative Total
Baseline Cost Plan		
Federal Share	179,899	4,093,126
Non-Federal Share	117,201	1,078,889
Total Planned	**297,101**	**5,172,015**
Actual Incurred Cost		
Federal Share	400,154	2,154,796
Non-Federal Share	161,310	1,438,118
Total Incurred Cost	**561,464**	**3,592,914**
Variance		
Federal Share	-220,255	1,938,330
Non-Federal Share	-44,109	-359,229
Total Variance	**264,363**	**1,579,101**

Please note that the PMP also has a spending plan that is based on calendar quarters.

8. **PROJECT OUTCOMES**
Nothing to Report.

9. REFERENCES

Dabbous, M.K. 1977. Displacement of Polymers in Waterflooded Porous Media and Its Effects on a Subsequent Micellar Flood. *SPE Journal* (October) 358-368.

Dawson, R., and Lantz, R.B. 1972. Inaccessible Pore Volume in Polymer Flooding. *SPEJ* **12** (5): 448–452.

Dominguez, J.G. and Willhite, G.P. 1977. Retention and Flow Characteristics of Polymer Solutions in Porous Media. *SPE Jour*nal (April) 111-121.

Jouenne, S., Heurteux, G., Haorcq, C., Joly, M., Questrel, M., Levache, B. 2019. Universal Viscosifying Behavior of Acrylamide-based Polymers Used in EOR—Application for Aq/QC, Viscosity Predictions and Field Characterization. 20th European Symposium on Improved Oil Recovery. 8-11 April.

Kang, Wanli, et al. "Demulsification performance, behavior and mechanism of different demulsifiers on the light crude oil emulsions." Colloids and Surfaces A: Physicochemical and Engineering Aspects 545 (2018): 197-204.

Knight, B.L., Jones, S.C., and Parsons, R.W. 1974. Discussion. *SPE Journal* (December) 643-644.

Liu, Yang, et al. "Study on emulsification behavior and optimized separation technology of high concentration polymer flooding produced liquid in Daqing Oilfield." SPE Middle East Oil & Gas Show and Conference. Society of Petroleum Engineers, 2015.

Lotsch, T., Muller, T., Pusch, G. 1985. The Effect of Inaccessible Pore Volume on Polymer Core Experiments. Paper SPE 13590 presented at the International Symposium on Oilfield and Geothermal Chemistry. Phoenix, AZ. 9-11 April.

Manichand, R.N., and Seright, R.S. 2014. Field vs Laboratory Polymer Retention Values for a Polymer Flood in the Tambaredjo Field. *SPE Res Eval & Eng*. **17**(3): 314-325 http://dx.doi.org/10.2118/169027-PA.

Pancharoen, M., Thiele, M.R., and Kovscek, A.R. 2010. Inaccessible Pore Volume of Associative Polymer Floods. Paper SPE 129910 presented at the SPE Improved Oil Recovery Symposium. Tulsa, OK. 24-28 April.

Shah, B.N., Willhite, G.P., and Green, D.W. 1978. The Effect of Inaccessible Pore Volume on the Flow of Polymer and Solvent through Porous Media. Paper SPE 7586 presented at the SPE Annual Technical Conference and Exhibition. Houston, TX. 1-3 October.

Seright, R.S. 2017. How Much Polymer Should Be Injected during a Polymer Flood? Review of Previous and Current Practices. *SPE Journal* **22**(1): 1-18. http://dx.doi.org/10.2118/179543-PA.

Vela, S., Peaceman, D.W., and Sandvik, E.I. 1976. Evaluation of Polymer Flooding in a Layered Reservoir with Crossflow, Retention, and Degradation. *SPE J.* **16** (2): 82–96. SPE-5102-PA. doi: 10.2118/5102-PA.

Zhang, Guoyin, and Seright, R.S. 2014. Effect of Concentration on HPAM Retention in Porous Media. *SPE Journal* **19**(3): 373-380. Paper 166256. http://dx.doi.org/10.2118/166256-PA.